Title

Extracellular vesicles from mouse trophoblast cells: Effects on neural progenitor cells and potential participants in the placenta—brain axis

Journal

Biology of Reproduction, 110(2)

ISSN

0006-3363

Authors

Kinkade, Jessica A

Seetharam, Arun S

Sachdev, Shrikesh

et al.

Publication Date

2024-02-10

DOI

10.1093/biolre/ioad146

Peer reviewed

Biology of Reproduction, 2024, **110(2)**, 310–328
https://doi.org/10.1093/biolre/ioad146
Advance access publication date 26 October 2023
Research Article

Extracellular vesicles from mouse trophoblast cells: Effects on neural progenitor cells and potential participants in the placenta–brain axis†

Jessica A. Kinkade[1,2], Arun S. Seetharam[3,4], Shrikesh Sachdev[2], Nathan J. Bivens[5], Brett S. Phinney[6], Gabriela Grigorean[6], R. Michael Roberts[2,*], Geetu Tuteja[4,*] and Cheryl S. Rosenfeld[1,7,8,9,*]

[1]Biomedical Sciences, University of Missouri, Columbia, MO, USA
[2]Division of Animal Sciences, University of Missouri, Columbia, MO, USA
[3]Department of Ecology, Evolution and Organismal Biology, Iowa State University, Ames, IA, USA
[4]Department of Genetics, Development and Cell Biology, Iowa State University, Ames, IA, USA
[5]Genomics Technology Core Facility, University of Missouri, Columbia, MO, USA
[6]Proteomics Core UC Davis Genome Center, University of California, Davis, CA, USA
[7]MU Institute of Data Science and Informatics, University of Missouri, Columbia, MO, USA
[8]Genetics Area Program, University of Missouri, Columbia, MO, USA
[9]Thompson Center for Autism and Neurobehavioral Disorders, University of Missouri, Columbia, MO, USA

*__Correspondence:__ R. Michael Roberts, Division of Animal Sciences, University of Missouri, Columbia, MO, USA. Tel:/Fax: (573) 239-4505; Geetu Tuteja, Tel:/Fax: (515) 294-3417; Cheryl S. Rosenfeld, Department of Genetics, Development and Cell Biology, Iowa State University, Ames, IA, USA. Tel:/Fax: (573) 882-5132. Thompson Center for Autism and Neurobehavioral Disorders, University of Missouri, El02 Veterinary Medicine Building, Columbia, MO 65211, USA. E-mail: rosenfeldc@missouri.edu

†__Grant Support:__ Research was supported with a University of Missouri Research Council Grant, National Institutes of Health (NIH) grants 1R01ES025547 (CSR) and R01HD094937 (RMR). The small RNA bioinformatics analysis was supported in part by R01HD096083 (to GT) and HPC@ISU equipment at Iowa State University (partially funded by National Science Foundation [NSF] under MRI grant number 1726447).

Abstract

The fetal brain of the mouse is thought to be dependent upon the placenta as a source of serotonin (5-hydroxytryptamine; 5-HT) and other factors. How factors reach the developing brain remains uncertain but are postulated here to be part of the cargo carried by placental extracellular vesicles (EV). We have analyzed the protein, catecholamine, and small RNA content of EV from mouse trophoblast stem cells (TSC) and TSC differentiated into parietal trophoblast giant cells (pTGC), potential primary purveyors of 5-HT. Current studies examined how exposure of mouse neural progenitor cells (NPC) to EV from either TSC or pTGC affect their transcriptome profiles. The EV from trophoblast cells contained relatively high amounts of 5-HT, as well as dopamine and norepinephrine, but there were no significant differences between EV derived from pTGC and from TSC. Content of miRNA and small nucleolar (sno)RNA, however, did differ according to EV source, and snoRNA were upregulated in EV from pTGC. The primary inferred targets of the microRNA (miRNA) from both pTGC and TSC were mRNA enriched in the fetal brain. NPC readily internalized EV, leading to changes in their transcriptome profiles. Transcripts regulated were mainly ones enriched in neural tissues. The transcripts in EV-treated NPC that demonstrated a likely complementarity with miRNA in EV were mainly up- rather than downregulated, with functions linked to neuronal processes. Our results are consistent with placenta-derived EV providing direct support for fetal brain development and being an integral part of the placenta–brain axis.

Summary Sentence

Extracellular vesicles (EV) from mouse trophoblast cells contain 5-HT and small RNA that might affect neural transcripts, and neuronal progenitor cells internalize and respond to such EV by changes in gene expression linked to neuron development.

Received: January 31, 2023. **Revised:** October 12, 2023. **Accepted:** October 21, 2023

Graphical Abstract

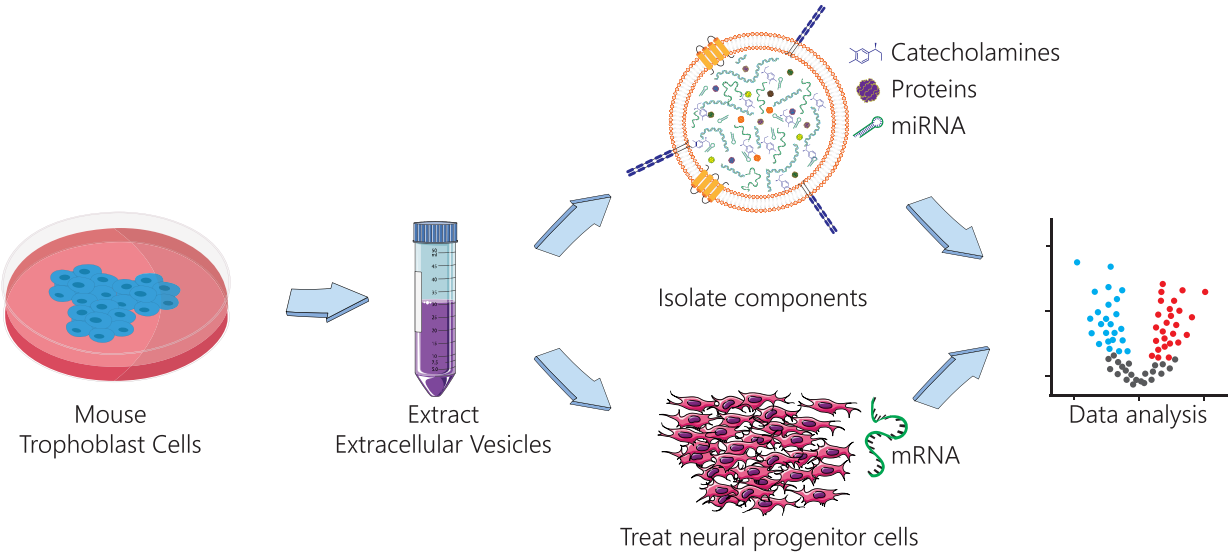

1 The arrow-curved-clockwise-3, arrow-curved-counterclockwise, falcon-50ml-pink, fibroblasts 1 to 5 icons by Servier https://smart.servier.com/ is licensed under CC-BY 3.0 Unported (https://creativecommons.org/licenses/by/3.0/).
2 The Protein-colored (modified) icon by the Database Center for the Life Sciences (DBCLS) is licensed under CC BY 4.0 (http://creativecommons.org/licenses/by/4.0).
3 The Stem cell colony icon by Marcel Tisch (Marcel.Tisch@uibk.ac.at) is licensed under CC-0.

Key words: placenta, placenta–brain axis, proteomics, neurotransmitters, serotonin, small RNAs

Introduction

The eutherian placenta serves as a vital link between the mother and fetus and is essential in exchange of gasses, nutrients, waste, hormones, and other factors. The placenta acts to regulate maternal physiological processes, including maintenance of the ovarian corpus luteum and prevention of an immune attack against the semi-allogenic fetus. In the mouse and probably also the human, the fetal brain is especially dependent upon the placenta [1, 2]. The close developmental link between the two organ systems is sometimes called the placenta–brain axis and demands further exploration. Doing so will help us better understand the origin of some of the neurobehavioral disorders that originate in utero.

The provision of the catecholamine serotonin (5-hydroxytryptamine, 5-HT) may provide an example whereby the placenta modulates fetal brain development. 5-Hydroxytryptamine is known to influence almost all essential neurological processes that span from glial formation to synaptogenesis [3–5]. 5-Hydroxytryptamine presence in the human placenta was first reported in 1965 [6] and has been an active topic of interest since then, but its role is uncertain. It even remains unclear whether 5-HT is synthesized in significant amounts by human placental trophoblast (TB) [7, 8], even though the capacity for its biosynthesis, catabolism, and uptake have been demonstrated in certain human TB cell types [9–13]. In the mouse, a comparison of E7.5 to 9.5 conceptuses indicates that the genetic machinery to produce 5-HT is upregulated [14, 15], and 5-HT immunoreactivity becomes visible in the ectoplacental cone (EPC) [16]. The junctional zone, which emerges from the distal end of the EPC between embryonic age E9 and 12, comprised primarily spongiotrophoblast, glycogen cells, and invasive secondary parietal trophoblast giant cells (pTGC) [17–19]. The latter, particularly those nearest decidual blood capillaries [16], stain strongly for 5-HT, as well as a second catecholamine, dopamine [20]. These cells have massively endoreduplicated DNA [21] and perform a vital endocrine function [22]. In the fully functional mature placenta seen at E12.5, pTGC form a narrow layer between the spongioTB and maternal decidua and specifically express the gene *Prl2c2*, which encodes the growth factor proliferin (PLF/PRL2C2) [22]. An apparent concentration gradient from the pTGC through the spongioTB has been proposed as a potential route for provisioning the fetus, especially the early brain, with 5-HT [23]. In this regard, there appears to be a progressive switch during brain development from an early placental source of 5-HT, which is vital for proper forebrain development, to a later endogenous source from the fetal brain itself [16, 23]. That early placental source has been proposed to be either 5-HT derived directly from the mother [8, 16, 24] and/or synthesized in the placenta at the expense of maternal tryptophan [10, 14, 23, 25, 26].

Recently, we found that developmental exposure to the endocrine-disrupting chemical, bisphenol A, affected placental miRNA profiles. We predicted that affected miRNA would most likely target mRNA associated with the placenta. However, the potential target mRNA appeared to be enriched in the thymus and various neural tissues rather than trophoblast [27]. Pathway enrichment analyses revealed that the targeted mRNA primarily regulated neurogenesis and associated pathways in the brain. Another mouse study that examined miRNA expression patterns in the placenta and brain likewise suggested that placental miRNA contribute to fetal brain development [28]. Ablation of the placental mammal-specific miR379–410 cluster in the mouse results in hypersocial behavior, increased excitatory synaptic transmission, and enhanced expression of ionotropic glutamate receptor complexes in the hippocampus [29]. The findings suggest that this placenta-specific miRNA cluster acts to modulate social

behaviors and excitatory impulses. A human cohort study showed correlations between placental miRNA and mRNA and intellectual and social impairments [30], providing further evidence that miRNA serve as another key link in the placenta–brain axis. The key question that arises from all these studies is: how do placental miRNA reach the brain intact to shape gene expression and thereby development of this organ? One possibility is that placental miRNA are transported to the brain as cargo of extracellular vesicles (EV) where they would be protected from degradation.

Based on their architecture and contents, EV are primarily categorized as microvesicles, exosomes, and apoptotic bodies. Exosomes are membrane-bound vesicles derived from cytoplasmic multivesicular bodies. They range in diameter from 30 to 160 nm [31] and contain proteins and lipids, as well as DNA, mRNA, and miRNA [31] that the EV are able to shuttle to remote target organs. Much of the work performed to date has examined how placenta-derived EV influence the mother during pregnancy or change with disease, for example, in preeclampsia and gestational diabetes [32–47]. No study to date, however, has examined the effects of placenta-derived EV on early fetal brain development or used in vitro approaches to study their effects on neural cells. If, in fact, EV do shuttle miRNA, catecholamines, and other molecules from the placenta to the emerging brain, future studies might provide insight into neurobehavioral disorders that trace their origins to the in utero period. For instance, alterations in fetal serotonin levels have been linked with autism spectrum disorders [1, 2, 48, 49].

Materials and methods

Differentiating pTGC in cell culture and collection of culture media

Mouse trophoblast stem cells (TSC) [50] were provided by Dr. Michael Soares (University of Missouri Kansas City, Kansas City, MO). These cells can be readily differentiated into pTGC [51]. The line we use is the prototype line generated by Kunath et al. that has been widely studied, contributes solely to placental trophoblast in chimeras, and gives rise readily to trophoblast giant cells [15, 50, 52–54]. The transcriptome profiles of both cell types have been well characterized [55]. We opted to use this cell line as our studies examining effects of bisphenols and oxycodone indicate that pTGC are vulnerable to xenobiotics in the in utero environment [20, 56].

Briefly, TSC were cultured on a layer of irradiated mouse embryonic fibroblasts (MEF) and passaged once a week (with 150 000 cells passaged onto each well of two 6-well plates of fresh MEF). To induce differentiation, 38 000 cells were passaged onto each well of four 6-well plates without MEF and were further cultured on a mixture of 70% MEF-conditioned TB medium and 30% regular TB medium lacking FGF4 and heparin but in the presence of retinoic acid (0.5 ml of 5 mM/ml) (Figure S1). Supplementing the medium with retinoic acid preferentially induced pTGC rather than other cell types [22]. Each plate was only partially composed of pTGC by day 6, as determined by the proportion expressing *Prl2c2* immunoreactivity (Figure S2), and the population of pTGC remains heterogeneous in size. In a revised protocol, undifferentiated TSC were passaged onto four 6-well plates without MEF at 600 000 cells/well and cultured for 2 days on a mixture of 70% MEF-conditioned TB medium and 30% regular TB medium with FGF4 and heparin to maintain an undifferentiated state. To avoid the presence of bovine exosomes, the culture medium (CM) was supplemented with exosome-free FBS. Media (CM) were harvested from undifferentiated TSC (day 2 for small RNA to increase the number of cells and D0 for catecholamine and proteomics analyses (cultured longer to help increase RNA yield) and differentiated pTGC (day 6). For those differentiated to pTGC, the medium was changed every other day during this 6-day period to minimize the likelihood of contamination from TSC-derived EV. For RNAseq analyses of EV, we ran four independent experiments per treatment group (8 total samples). Samples for proteomics and catecholamine analyses had five independent replicates per treatment group (10 total samples).

EV isolation from culture media for proteomics and neurotransmitter analyses

Extracellular vesicles were isolated by using an EV isolation kit (ExoQuick-TC ULTRA EV Isolation Kit for Tissue Culture Media; System Biosciences, Palo Alto, CA, USA), as per the manufacturer's protocol.

Transmission electron microscopy

Transmission electron microscopy (TEM) was used to determine EV morphology, suspension purity, and size (~50–1000 nm). Extracellular vesicles were processed on copper formvar/carbon grids (Electron Microscopy Sciences, Hatfield, PA), fixed in 2% (w/v) paraformaldehyde, and counterstained with uranyl acetate. Grids were viewed with a Jeol JEM-1400 Transmission Electron Microscope (Jeol USA Inc., Peabody, MA) connected to a Gatan Rio 9 camera (Pleasanton, CA).

Nanoparticle tracking analysis

Culture medium-containing EV from the different placental cultures were diluted 1:10 in 0.1 mm filtered PBS and their size, concentration, and Brownian motion analyzed with a NanoSight NS300 (Malvern Panalytical, St-Laurent, Quebec, CA). Five 60-s videos were processed with the NTA software (NanoSight) to track each particle.

Proteomics analysis of EV from pTGC and TSC

Sample preparation

Exosomes were lysed directly in 200 μl solubilization buffer (5% w/v aqueous sodium dodecyl sulfate, 50 mM triethyl ammonium bicarbonate) via sonication (Qsonica Q125, Newton, CT) (three rounds of alternating 10 s on/10 s off at 20% amplitude). Protein concentration was measured by a bichinoic acid assay (Thermo Scientific, USA). The proteins were subjected to reduction/alkylation/tryptic proteolysis by using suspension-trap (ProtiFi) devices. S-Trap is a powerful filter-aided sample preparation method that consists of trapping acid-aggregated proteins in a quartz filter prior to enzymatic proteolysis. The exosome lysate was directly loaded onto the S-Traps. Disulfide bonds were reduced with dithiothreitol and alkylated (in the dark) with iodoacetamide in 50 mM TEAB buffer. Digestion was with a first addition of trypsin 1:100 enzyme/protein (w/w) for 4 h at 37°C, followed by a boost addition of trypsin using same w/w ratios for overnight digestion at 37°C. To stop the digestion, the reaction mixture was acidified with 1% trifluoroacetic acid. The eluted tryptic peptides were dried in a vacuum centrifuge and re-constituted in water with 2% acetonitrile (ACN).

Liquid chromatography–mass spectrometry

Liquid chromatographic peptide separation was performed on an ultra-high-pressure nano-flow Easy nLC (Bruker Daltonics, Bremen, Germany). Flow rate of buffers was 0.85 μl/min, on a PepSep 150 μm × 25 cm C18 column (PepSep, Denmark) with 1.5 μm 100 Å pores, heated to a constant temperature of 40°C; nanoESI via a ZDV spray emitter (Bruker Daltonics). Mobile phases A and B were water with 0.1% formic acid (v/v) and 80:20:0.1% acetonitrile (ACN)/water/formic acid (v/v/vol), respectively. Peptides were separated by using a 35-min gradient: from 0 to 2 min increase buffer B to 5%, 2–5 min 5–10% B, 5–28 min 10–36% B, and 28–35 min 80% B—direct elution into the mass spectrometer. MS was performed on a hybrid trapped ion mobility spectrometry–quadrupole time-of-flight mass spectrometer (timsTOF Pro; Bruker Daltonics) with a modified nano-electrospray ion source (CaptiveSpray; Bruker Daltonics). In the experiments described here, the mass spectrometer was operated in diaPASEF mode. Desolvated ions entered the vacuum region through the glass capillary and deflected into the TIMS tunnel, which is electrically separated into two parts (dual TIMS). Here, the first region is operated as an ion accumulation trap that primarily stores all ions entering the mass spectrometer, while the second part performs trapped ion mobility analysis. Data-independent analysis (diaPASEF) was performed on a nanoElute UHPLC coupled to a timsTOF Pro. The acquisition scheme used for data-independent acquisition (DIA) consisted of four 25 m/z precursor windows per 100 ms TIMS scan. Windows began at 400 m/z and continued to 1200 m/z. The collision energy was ramped linearly as a function of the mobility from 63 eV at 1/K0 = 1.5 Vs cm^{-2} to 17 eV at 1/K0 = 0.55 Vs cm^{-2}.

Proteomics data analysis

Quantitative and statistical analysis was performed with the Spectronaut software. A decoy false discovery rate (FDR) at <1% for peptide spectrum matches and protein group identifications was used for spectra filtering (Spectronaut default). Decoy database hits, proteins identified as potential contaminants, and proteins identified exclusively by one site modification were excluded from further analysis. The proteomics data that were processed with Spectronaut with normalized values and fold change were downloaded as a CSV file (Core facility website). These data were used with custom R scripts to generate a principal component analysis (PCA) plot and volcano plot for all samples. The differentially expressed proteins were used for enrichment analyses, with TissueEnrich (v 1.16.0) and the Mouse ENCODE [57] reference set [58]. The Bruker LCMS DIA files were converted into htrms files with the htrms converter (Biognosys); parameters were set to default. The htrms files were analyzed with Spectronaut (version: 14.0.200601.47784; Biognosys) by using direct DIA. The UniProt database of reviewed *Mus musculus* proteins (accessed 08/04/2022) from UniProt, UP000000589, and a database of 112 common laboratory contaminants (https://www.thegpm.org/crap/) were used to identify peptides. A maximum of two missing trypsin cleavage sites were permitted per protein; the required minimum peptide sequence length was seven amino acids, and peptide mass was limited to a maximum of 4600 Da. Carbamidomethylation of cysteine residues was set as a fixed modification, and methionine oxidation and acetylation of protein N termini as variable modifications.

Functional enrichment analysis of proteins and their encoding genes differentially expressed between pTGC and TSC

Protein–protein interactions (PPI) for proteins differentially expressed between pTGC and TSC were determined with the STRING Database version 11.5 [59]. The PPI files generated with STRING were imported into the cytoHubba app [60] in Cytoscape [61] to examine the top 10 hub genes. Within this program, hub genes were determined with Maximal Clique Centrality (MCC) analysis, as recommended [60]. For functional enrichment analysis, DEG were imported in g:GOSt (https://biit.cs.ut.ee/gprofiler/gost), and the significance threshold used was FDR ≤0.01 (calculated by the Benjamini–Hochberg method). The output included all significant GO terms and pathways (KEGG, Reactome, and WikiPathways).

Catecholamine analyses of EV released from pTGC and TSC

To permit LC–MS analysis of catecholamines, serially diluted solutions ($n = 9$) were prepared as internal standards (IS) for each of the six targeted compounds in 70% acetonitrile. Each standard compound carried six deuterium atoms. For each EV sample, 50 μl volume was mixed with 50 μl of IS solution and 900 μl of water. The mixture was then loaded onto a reversed-phase solid-phase extraction cartridge. After discarding the flow-through fraction under positive pressure, the retained compounds were eluted with 1 ml of methanol. The collected fraction was dried under a nitrogen gas flow and the residue re-constituted in 50 μl of 70% acetonitrile and mixed with 50 μl of 20 mM dansyl chloride solution and 50 μl of borate buffer. The mixtures were allowed to react at 40°C for 60 min. After the reaction, 10 μl of each solution was injected into a UPLC-MRM/MS on a Waters Acquity UPLC system coupled to a Sciex QTRAP 6500 Plus mass spectrometer with positive-ion detection. LC separation was conducted on a C18 UPLC column (2.1 × 150 mm, 1.8 μm) with 0.1% formic acid in water and 0.1% formic acid in acetonitrile as the binary solvents for gradient elution (50% to 100% B in 15 min) at 50°C and 35°C. Concentrations of detected compounds were calculated by reference to internal standard values by interpolating the constructed linear-regression curves of individual compounds with the analyte to internal standard peak ratios.

Small RNA isolation from EV and small RNA sequencing

MicroRNA and mRNA were isolated with EVeryRNA EV RNA Purification System that includes the ExoQuick-TC EV Isolation (Systemic Biosciences). Samples were analyzed on the fragment analyzer at the MU Genomics Technology Core Facility, and only those samples with a RQN score >7 were used to construct libraries for sequencing.

Small RNA library preparation for EV from pTGC and TSC

Small RNA libraries were constructed with reagents supplied in the New England Biolab NEBNext small RNA library preparation kit. Briefly, a two-step ligation process was performed with total RNA to add adapters to the 3′ and 5′ ends of the small RNA, respectively. The adapter-modified small RNA was then reverse transcribed by using ProtoScript II Reverse Transcriptase followed by PCR to amplify and enrich the

small RNA libraries. These were pooled and then processed on Axygen AxyPrep MAG purification beads to perform a double-sided size selection (1.25×/1.50×) to remove adapter dimers and recover the desired insert size of 18–45 bases. The DNA fragments (libraries) were recovered by elution from the 1.5× beads binding fraction in 30 μl of Qiagen EB buffer. The DNA content of the final library pool was measured with the Qubit HS DNA kit and the fragment size analyzed by an Agilent Fragment Analyzer Automated CE system. Libraries were diluted according to Illumina's standard sequencing protocol for sequencing on the NovaSeq 6000 (Illumina).

Small RNAseq data processing and analysis

Raw reads were downloaded from the Genomics Technology Core, University of Missouri via the Wget command, and libraries for the same samples were concatenated, preserving the pairs. The initial quality screening was done by using the FastQC (v 0.11.9) program (http://www.bioinformatics.babraham.ac.uk/projects/fastqc/.). The mouse reference genome (version GRCm39), in fasta format, and annotation, in gtf format, were downloaded from Gencode [62]. STAR (v 2.7.10a) was used for mapping the reads [63]. The reference genome was indexed (runMode genomeGenerate) and sample pairs mapped individually. The presence of adapters, as indicated by the initial FastQC screening, necessitated adding options clip3pAdapterSeq (AGATCGGAAGAGC) and clip3pAdapterMMp (max proportion of mismatches in the adapter, set to 0.1) for mapping. The output was written as coordinate-sorted BAM files, after filtering with the final mappings by using STAR's output filtering options, as follows: the maximum number of multi-mapping was limited to 20; the ratio of mismatches to the mapped length was set to 0.03; the alignment score based on normalized read length (paired) was set to 0; the minimum number of matched bases required was set to 16. The overhang for spliced alignments was disabled by setting alignSJDBoverhangMin to 1000, as there could be many unannotated small RNA. The maximum intron size was set to 1, allowing a longer split mapping of reads. The count table for all the "gene" features in the gtf file were computed by the quantMode (set to GeneCounts) option. Apart from these options, we also included other parameters to optimize runtime or resource usage.

The count tables for individual samples were joined by bash scripting and were filtered to retain only features of biotype miRNA, miscRNA, scRNA, snRNA, snoRNA, and scaRNA for all samples. Differential gene expression analyses of small RNA were carried out by DESeq2 (v 1.36.0) [64]. Briefly, gene counts were prefiltered to retain features with total counts of greater than 5 across all the samples, normalized by variance stabilizing transformations (vst), and evaluated for differential expression (DE) with the Wald statistical test. The built-in functions of DESeq2 were used to create a sample heatmap and, for PCA, to visualize the consistency of replicates (by using the top 1000 variable genes). The DE gene list was generated after filtering them according to an adjusted *P*-value $\leq$0.05 and absolute fold change $\geq$1.5. A heatmap for the 30 most variable features (small RNA genes) was generated with the pheatmap (v 1.0.12) package [65]. The most highly expressed small RNA in each condition (the top quartile according to normalized DESeq2 expression values) were further compared.

The target genes for DE miRNA genes were obtained by means of the https://mirdb.org/ database [66, 67], and the overlap of the target genes in both conditions was inspected by using a Venn plot. The https://mirdb.org/ database allows identification of target genes for each miRNA. We downloaded the file from the server and linked each miRNA from our lists to their targets. The information downloaded from the server had score information and for many other species. A filtered list of just mouse, with score $\geq$80, was created. The target gene ids were in RefSeq format, which was converted to gene symbol. Based on the predicted mRNAs, we then performed enrichment analyses with enrichr, using the DisGeNET (version 7.0) database [68] and KEGG (mouse 2019) libraries [69, 70]. Tissue-specific gene enrichment analyses were carried out with the TissueEnrich (v.1.16.0) Bioconductor package with the Mouse ENCODE [52] reference set [58].

Exposure of mouse neural progenitor stem cells to EV from pTGC and TSC and RNA isolation from NPC

These studies used mouse cortical neural stem cells (NSC, Cat # SCR 029; Sigma Chemical, St. Louis, MO) that represents primary neural stem cells isolated from the cortices of embryonic days 15–18 (E15–E18) C57/BL6 mice. Cells were cultured in mouse Neural Stem Cell Growth Medium (Cat M813-250; Sigma Chemical) until they achieved 75% confluence. Mouse NSC were treated with EV from TSC or pTGC labeled with Invitrogen BODIPY TR Ceramide (ThermoFisher Scientific, St, Louis, MO) based on the manufacturer's protocol. In total, 20, 40, and 60 min after EV application, the NPC were fixed with 4% PFA, permeabilized with 0.1% triton (5 min), and stained with Alexa Fluor 488 Phalloidin (Invitrogen cat #A12379), as per the recommendations provided with the kit. Cells were than analyzed with a Leica TCS SP8 confocal system (Leica Biosystems, Deer Park, IL) (Figure 9A and B). Fluorescent images were obtained and 3D video animation of these cells acquired with LAS X software program (Figure 9C through H and Videos 1 and 2).

For the transcriptome studies, mouse NPC were exposed for 24 h to EV from TSC, EV from pTGC, or media alone, and cells were then harvested. Ribonucleic acid was isolated from mouse NPC treated with EV from TSC or pTGC or media alone (control) with the Qiagen AllPrep DNA/RNA/miRNA Universal Kit (Catalog #80224; Qiagen, Germantown, MD). The quantity and quality of the RNA was determined with a Nanodrop ND1000 spectrophotometer (Nanodrop Products, Wilmington, DE). The results were further confirmed by analyzing the RNA on the Fragment Analyzer (Advanced Analytical Technologies, Ankeny, IA). Only those samples that had an RIN score >8.0 were selected for RNA sequencing (RNAseq).

Illumina stranded mRNA library preparation and sequencing for NPC RNA

Libraries were constructed per the manufacturer's protocol with reagents supplied in Illumina's Stranded mRNA Library Preparation, Ligation Kit and sequenced at the University of Missouri Genomics Technology Core. In brief, poly-A containing mRNA was purified from total RNA using poly-T oligo beads, mRNA was fragmented, and double-stranded cDNA was generated from cleaved RNA using random hexamers. Pre-index anchors were ligated to the ends of cDNA. A subsequent PCR step was used to selectively amplify the anchor-ligated DNA fragments and add indexes and primer

sequences for cluster generation. The final amplified cDNA constructs were purified by addition of AxyPrep Mag PCR Clean-up beads. Unique dual indexing was used to mitigate index hopping events known to be an issue on patterned flow cells with exclusion amplification chemistry.

The size and purity of the final library was determined using the Fragment Analyzer (Agilent Technologies, Inc.), quantified with the Qubit fluorometer by means of the Qubit dsDNA HS Assay kit (Invitrogen), and diluted according to Illumina's standard sequencing protocol. Libraries were pooled and run on an Illumina NovaSeq 6000 sequencer using a paired-end 100-bp read format on a S4 flow cell to generate 50 million paired reads per sample. The actual number of reads obtained for each sample is listed in Table S1.

RNAseq data processing

Data were downloaded from the sequencing facility webserver via a secure rsync protocol and analyzed following standard procedures (see Supplemental Methods). FastQC (v0.11.7) [71] was employed to check the quality of the downloaded files and to obtain the average read length for each library. The fastq files were mapped to a STAR (v2.5.3a) [63] indexed mouse reference (GRCm39) [62] that was generated by using the mode genomeGenerate (—runMode genomeGenerate) and with GTF file (—sjdbGTFfile). The Gencode vM30 GTF file was used for gene annotations. Read mapping was performed by using the mode alignReads (—runMode alignReads) and was optimized for short reads with the options "—outFilterScoreMinOverLread 0.3" and "—outFilterMatchNminOverLread 0.3." The individual bam files of each sample file were used with featureCounts from the subread package to generate a combined count file. The count file was filtered to retain only protein-coding genes. The quality control reports from all the pre-processing steps were compiled by MultiQC [72].

The raw count files were imported into R and analyzed to obtain differentially expressed genes by using DESeq2 (v1.30.1) [73]. Specifically, we retained the genes with counts greater than 10 across all conditions and evaluated for differential expression with the Wald statistical test. The resulting *P*-values were corrected for multiple testing with Benjamini–Hochberg [74] to control the FDR. Differentially expressed genes were identified after filtering them according to a *P*-value (adjusted) ≤ 0.05 and absolute fold change ≥ 1.5. Enrichment analyses were carried out using TissueEnrich [58], using the mouse ENCODE dataset [75], and also using EnrichR [76] with KEGG_2019_Mouse database.

Results

General features of trophoblast EV

We analyzed the EV isolated from mouse TSC and pTGC cells via TEM and found that they each exhibited typical membrane-bound structures spanning a range of sizes (Figure S3). NanoSight analysis was used to confirm the mean number and concentration of EV isolated, and the information was used to guide proteomics and small RNAseq analyses. A representative sample is shown in Figure S3. Based on the NanoSight analysis, the average EV concentration isolated from similar amounts of starting cells was 140 600 000 ± 31 907 909 particles/ml for pTGC and 257 400 000 ± 124 048 216 particles/ml for TSC. The average size of each particle was 104.72 ± 9.48 nm for TGC and 104.10 ± 10.86 nm for TSC.

Proteomics analyses of EV released from pTGC and TSC

We compared the protein profiles of TSC and pTGC and found distinct clustering based on 2D principal component analyses, with TSC replicates forming one cluster (shown in green in Figure 1A) and pTGC replicates forming a second and distinct cluster (shown in pink in Figure 1A). Comparison of the two groups revealed several proteins that differed significantly between the two groups based on a *q* value ≤ 0.05. Data are presented in the volcano plot shown in Figure 1B. Among the differentially expressed proteins were several heat shock proteins, e.g., HSP90AA1, HSPAB1, HSPA11, and HSPA8, and keratin family members, e.g., KRT10, KRT13, KRT14, KRT16, and KRT17. A full list of differentially expressed proteins is provided in Supplementary File S1. In this file, NaN (not applicable number) means the protein was identified but not quantified.

Input of proteins upregulated in pTGC into the TissueEnrich program [58] reveals that the genes encoding them are significantly enriched for genes with liver-specific expression (Figure 2A). However, there were others encoding proteins with placenta-enriched expression, including *Hspb1*, *Anxa11*, *Anxa8*, *Hspg2*, *Alpl*, *A2m*, *Tgm2*, and *Lgals3* (Figure 2B). For proteins upregulated in EV derived from TSC, there was no significant enrichment for tissue-specific gene expression (Figure S4). The only gene with placenta-enriched expression, which also had brain-enriched expression, was *Hbby*, a fetal hemoglobin. STRING analyses of the differentially expressed proteins reveals one large cluster and another smaller cluster (Figure S5). The top 10 hub proteins, meaning that they are in the center of the main interactions/networks, are various forms of keratin (Figure S5).

Based on Gene Ontology Cellular Component terms, many of the proteins in the analyzed EV, including those that differed between TSC and pTGC, were typical of extracellular vesicles, extracellular organelles, and extracellular exosomes (Figure S6). Based on Gene Ontology Biological Process analysis, they have also been linked to tissue and epithelial development. Geno Ontology Molecular Function indicates that the proteins are typically associated with cell adhesion and cadherin binding. Pathway analyses suggest some association to estrogen signaling, biosynthesis of amino acids, carbon metabolism, proteasome, keratinization, immune system, and cell response to stress (Figure S7). The full list of GO terms and pathways based on these differentially expressed proteins is provided in Supplementary File S2.

Catecholamine analyses of EV released from pTGC and TSC

Liquid chromatography–mass spectrometry (LC–MS) analyses identified serotonin (5-HT), dopamine, and norepinephrine in EV from undifferentiated and differentiated mouse TB cells. However, the amount of these catecholamines was quite variable and did not differ significantly between EV released from TSC and pTGC (Figure 3). Note, however, that the concentration of 5-HT (pTGC: 50 ± 11.9 nM and TSC: 131.6 ± 23.3 nM) was almost two orders of magnitude greater than that of dopamine and ~300-fold higher than that of norepinephrine in both cell types.

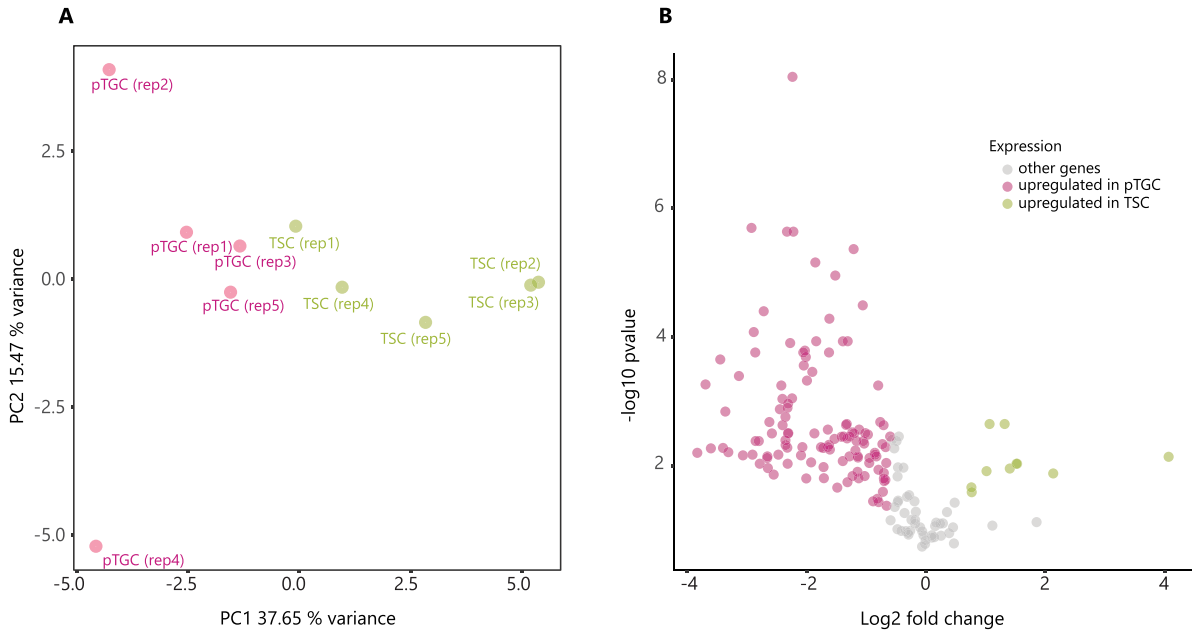

Figure 1. Plots for differentially expressed proteins contained within EV released into the culture media from undifferentiated (trophoblast stem cells, TSC) and differentiated cells (parietal trophoblast giant cells, pTGC). (A) 2D PCA plot with EV derived from TSC replicates shown in green and pTGC replicates shown in pink. EV from TSC formed one cluster and the pTGC replicates formed a second cluster. (B) Volcano plot showing several differentially expressed proteins between undifferentiated and differentiated TB cells. Pink dots represent proteins upregulated in EV from pTGC cells, and green dots are proteins upregulated in EV from TSC. Five independent replicates were used for both cell types.

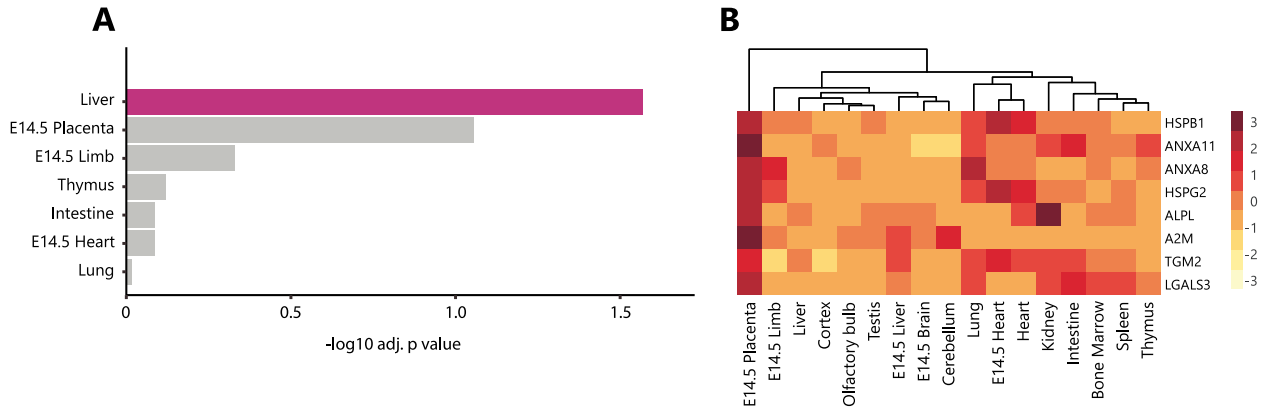

Figure 2. TissueEnrich analysis of proteins upregulated in EV derived from pTGC. (A) Bar graph shows that genes encoding the proteins upregulated in pTGC are significantly enriched for liver-specific expression. (B) Heat map shows genes with placenta-enriched expression encoding proteins enriched in EV from pTGC. These include *Hspb1*, *Anxa11*, *Anxa8*, *Hspg2*, *Alpl*, *A2m*, *Tgm2*, and *Lgals3*.

Small RNAseq analyses of small RNA in EV released from pTGC and TSC: general features

The PCA plot revealed relatively good separation between small RNA expressed in EV derived from pTGC, which clustered tightly, and those from TSC (Figure 4A). The volcano plot (Figure 4B) and heat map (Figure 5) confirm that the complement of small RNA in the two kinds of vesicle differed. The heat map, in particular, which shows that among the top 30 most variable small RNA, i.e., those with the greatest differences in expression between the two types of EV, there was distinct clustering based on whether the EV were derived from pTGC or TSC. For example, nine miRNA highly expressed in the TSC were present at extremely low levels after differentiation to pTGC. Only one miRNA in this set, *Mir135b*, showed the reverse change, namely, upregulation after differentiation. The remaining 20 small RNA of the 30 most variable were predominantly snoRNA, all of which generally demonstrated low abundance in TSC and marked upregulation in pTGC. We speculate that these snoRNA reflect expression of early genes in the differentiation trajectory. The full list of differentially expressed small RNA is provided in Supplementary File S3, with those upregulated in pTGC listed in one tab and those upregulated in TSC in another tab within the file.

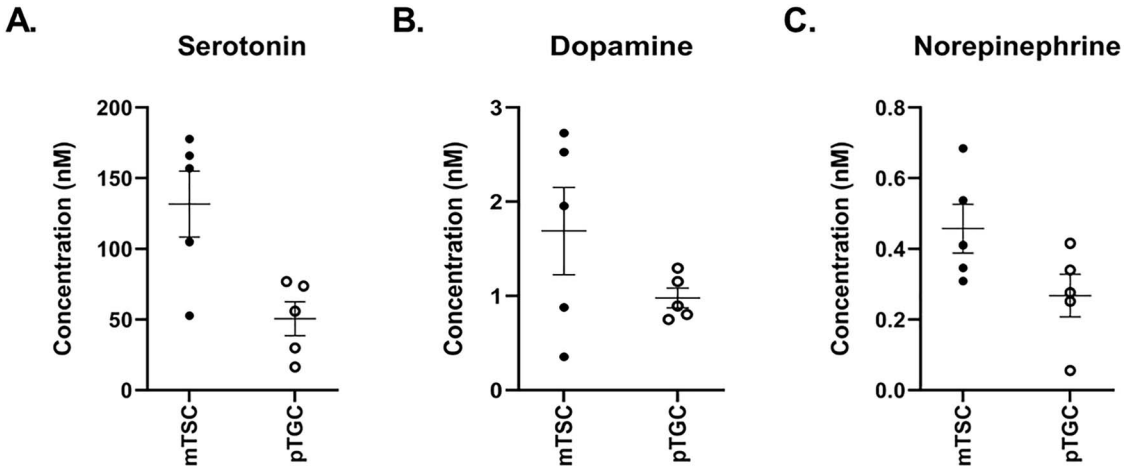

Figure 3. LC–MS analyses of catecholamines contained with EV derived from TSC and pTGC. No differences were detected for serotonin (5-HT), dopamine, and norepinephrine between the two groups. As shown, 5-HT was the most abundant catecholamine identified in EV from both TB groups. Five independent replicates were assessed for each group. Graphs represent the average ± standard error of the mean (SEM).

As alluded to above, smallRNAseq identified several classes of small RNA in addition to miRNA. These included miscellaneous RNA (miscRNA), small nuclear RNA (snRNA), small nucleolar RNA (snoRNA), and small activating RNA (scaRNA), which are believed to target gene promoters to induce transcriptional gene activation. As shown in Figure 6A, which compares the most highly expressed small RNA (top quartile) between TSC and pTGC, 225 (93.0% of the top quartile TSC small RNA and 71.7% of the top quartile pTGC small RNA) were present in both cell types. These were largely miRNA and snoRNA. The pTGC possessed 89 (28.3%) small RNA transcripts that were not in the top quartile of TSC-expressed small RNA. Again, these were mainly snoRNA and miRNA, but with a considerable proportion of snRNA also present. About one-half the snoRNA (35 of 69) that were only identified in the top quartile of small RNA in pTGC have not been classified on a functional basis (Figure 6B). Another 28 are of the C/D box class that form methylating and non-methylating ribonucleoprotein complexes class; five are of the H/ACA box class that are believed to guide pseudouridyl modifications in their targets. The analysis also revealed one Cajal body-specific form (Figure 6B). Finally, only 17 (7.0%) transcripts were identified uniquely in the top quartile of TSC-expressed small RNA; all belonged to the miRNA class.

Target mRNA for miRNA within EV from pTGC and TSC

Since miRNA can regulate gene expression by pairing with particular mRNA, usually in their 3′ termini, the https://mirdb.org/ database [66, 67] was then used to predict the target transcripts of the differentially expressed miRNA in EV from pTGC and TSC, respectively (Supplementary File S3). For the miRNA present in pTGC EV, a total of 5809 mRNA can be predicted as possible targets, with 1221 being unique targets to miRNA present in EV from pTGC (Figure S8). As anticipated, for the miRNA present in TSC, an even larger number (9732) of potential target mRNA were identified, with 5144 being unique targets to miRNA in EV from TSC (Supplementary File S3). However, it is striking that 4588 mRNA are common potential targets for miRNA differentially expressed in either group of EV.

Tissue source for target mRNA for miRNA within EV from pTGC and TSC

The TissueEnrich program [58] was then used to determine which organs of the mouse have an abundance of transcripts that might be recognized by miRNA upregulated in the two types of EV. As shown in Figure 7A, the transcripts targeted by miRNA upregulated in EV derived from pTGC are significantly enriched for genes with tissue-specific expression in embryonic 14.5 brain, cerebellum, cortex, and olfactory bulb. Essentially identical results were obtained with the target mRNA for miRNA upregulated in TSC and when the overlapping miRNA targets from both EV sources were analyzed (Figure 7B and C).

While the miRNA populations within the pTGC and TSC EV were not identical, as mentioned previously, they plainly had the potential to target a similar complement of transcripts, as is evident from the heat maps shown in Figure 7D–F. Here, the top 25 most abundant mRNA in E14.5 brain that are likely to interact with the miRNA in EV are shown on the *y*-axis of each heat map, while the various organ systems that express these mRNA are represented on the *y*-axis of the heat map. Of the total mRNA targets identified by the TissueEnrich program as having brain-specific expression (578 for miRNA upregulated in TSC and 403 for miRNA upregulated in pTGC), 353 overlapped, i.e., they were likely targeted by miRNA upregulated in both sources of EV. A total of 225 mRNA with brain-specific expression were only predicted to be targeted by uniquely TSC miRNA, and 50 mRNA by uniquely pTGC miRNA (Supplementary File S3, tab titled "Target genes_BrainEnriched"). The inferred functions of the top brain-specific gene products affected by the actions of miRNA from pTGC are listed in Table 1.

These data confirm our earlier results, namely, (1) that the E14 fetal brain and its various component neural tissues are the richest source of transcripts with likely affinity for the EV miRNA, whereas other organs systems, such heart or liver, are

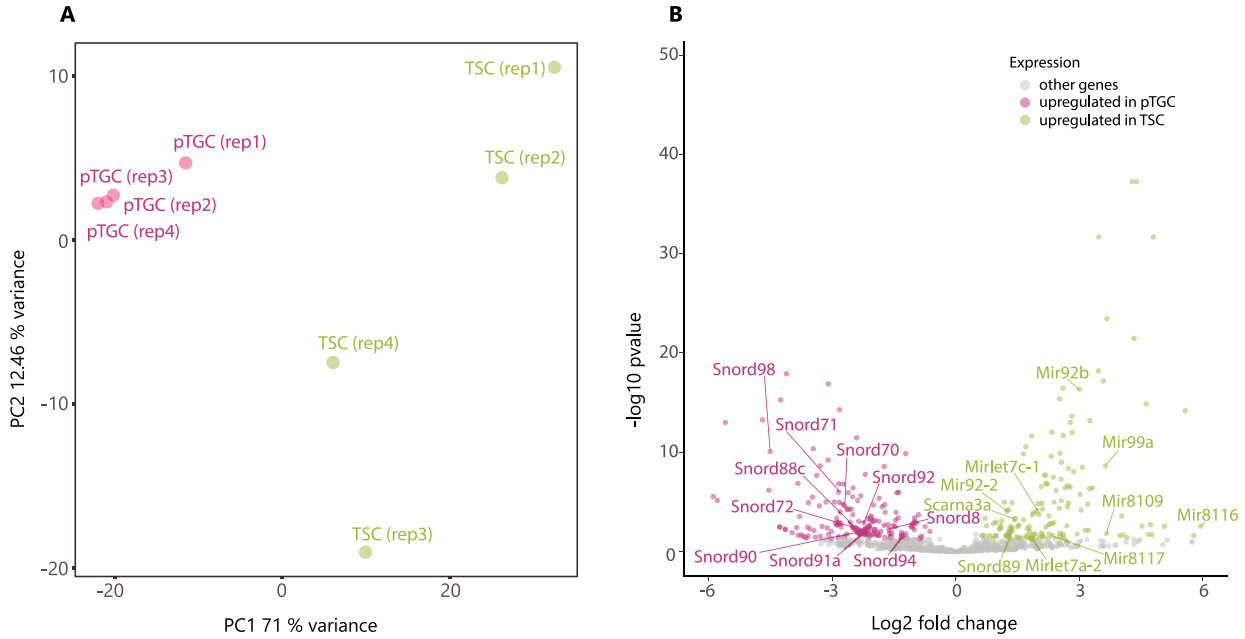

Figure 4. 2D PCA plot and volcano plot of small RNA in EV derived from differentiated TB cells (pTGC), and undifferentiated TB cells (TSC). (A) 2D PCA plot of small RNA from EV derived from pTGC (each pink circle represents one replicate) and TSC (each green circle represents one replicate). (B) Volcano plot of differentially expressed small RNA in EV. Those shown in pink are upregulated in EV derived from pTGC, whereas those upregulated in TSC are shown in green. Four replicates were tested for each cell type.

Table 1. Probable functions of gene products encoded by mRNA targeted by miRNA from EV of pTGC

DRP2	Maintenance of membrane-associated complexes at cellular connections
CTTNBP2	Regulates dendritic spine distribution
GABRA2	Ligand-gated chloride channel, GABA receptor, inhibitory neurotransmitter functions
NKX2-1	Regulates expression of genes involved in morphogenesis
AIF1L	Actin binding protein and promotes actin bundling
GRIK3	Glutamate receptor acting on ligand-gated ion channels
NCAN	Modulates neural adhesion and neurite growth
IKZF4	Transcriptional repressor
ELAVL3	Involved in neuronal differentiation and maintenance
PAX2	Transcriptional factor regulating CNS development

poor sources. (2) The EV from pTGC and TSC target many of the same of transcripts. For example, *Nnat*, *Stmn1*, and *Basp1*, each abundantly expressed in the brain, constitute the top three genes whose transcripts are most likely to interact with miRNA from both sources of EV.

Diseases associated with target mRNA for miRNA within EV from pTGC and TSC

Based on the predicted mRNAs, we then performed enrichment analyses with enrichr, using the DisGeNET (version 7.0) database [68] and WikiPathways (mouse and human, 2019) libraries [77] to screen for potential human-relevant diseases associated with such target mRNA. Diseases associated with mRNA targets for miRNA within EV from pTGC were almost all neurobehavioral disorders (Figure 7G), as were mRNA targets of miRNA within EV from TSC (Figure 7H) and when EV from pTGC and TSC were considered together (Figure 7I).

Internalization of EV derived from TSC and pTGC by mouse NSC

The above findings implicate a role for the EV contents affecting NPC differentiation. Consequently, we sought next to determine if EV from TSC and pTGC are internalized by mouse NPC and whether exposure to EV would affect the transcriptome profile of the targeted cells. EV from pTGC and TSC were fluorescently labeled and counted under the confocal microscope (Figure 8A and B). Subsequently, we exposed NPC to ~211 000 to 398 000 EV/well from pTGC and TSC and imaged the cells at 20 min, 40 min, and 60 min following these treatments. By 20 min post-exposure to EV from both TSC and pTGC, red fluorescence was visible within the cells and appeared to be concentrated in perinuclear location. The amount of fluorescent label appeared greater at 40 min and 60 min than it had been at 20 min, suggesting that internalization was a continuous process (Figure 8C and H, Videos 1 and 2).

General features of the transcriptome profile of NPC following exposure to EV from TSC or pTGC

For the transcriptome studies, NPC were exposed to similar concentrations of EV as listed above. The cells were harvested 24 h post-exposure, RNA isolated, and RNAseq performed. The average number of reads for all samples was 67 643 843, average percent alignment 91.0%, and average number of mapped reads 61 807 049 (Table S1). The 2D PCA plot reveals some separation between control NPC, those treated with TSC-derived EV, and those treated with pTGC EV (Figure S9A). Differential expression analysis revealed that if fairly stringent criteria were applied (adjusted *P*-value (p-adj) ≤ 0.05 and fold change ≥ 1.5), more genes were upregulated with EV treatment than were suppressed, and more transcripts were affected by EV from pTGC than TSC (222 vs. 88 transcripts, Figure S9B and C, Supplementary File S4).

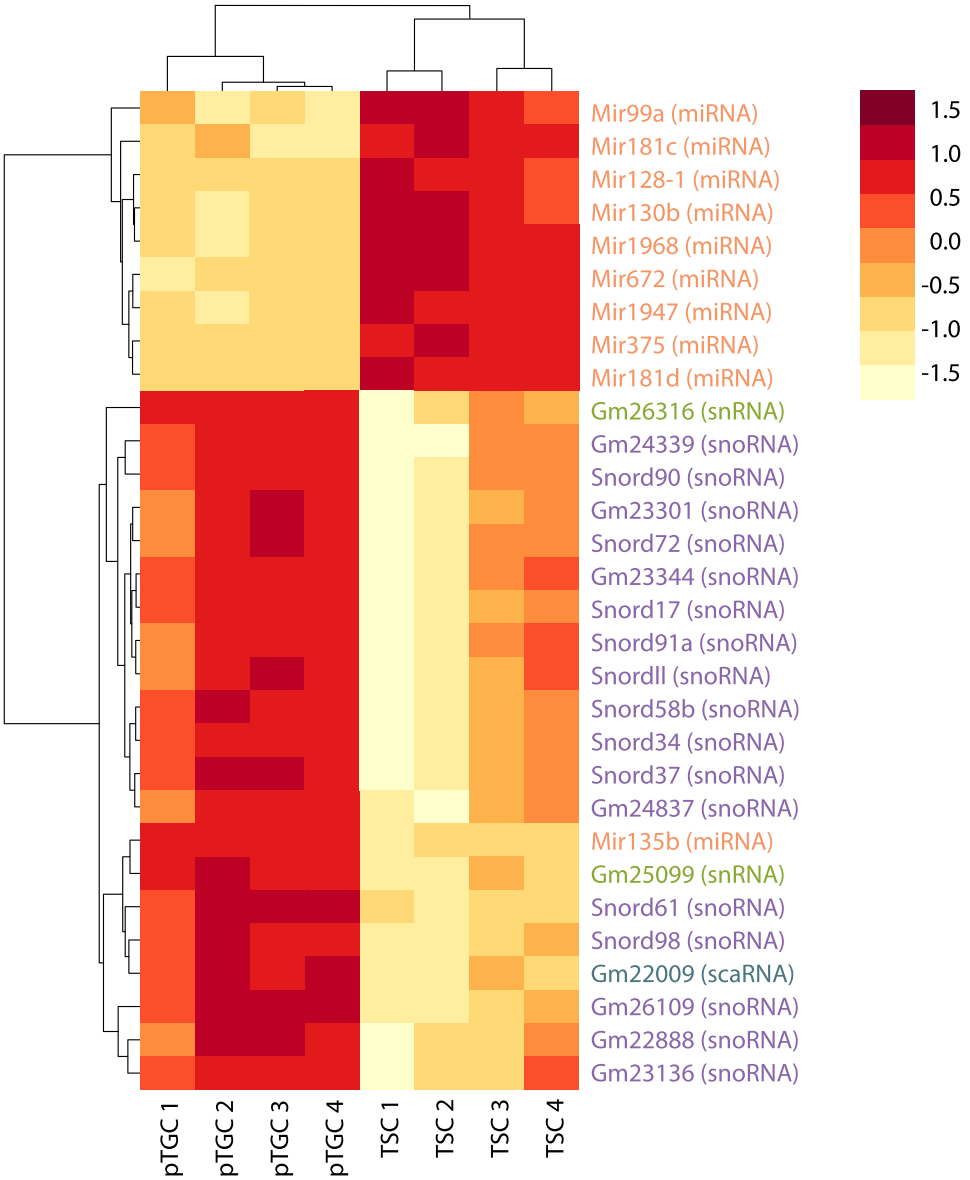

Figure 5. Heat map of the top 30 differentially expressed small RNA in EV derived from pTGC and TSC.

Differentially expressed genes in NPC induced by EV from TSC or pTGC

Venn diagram visualization of transcripts altered in NPC treated with pTGC EV or TSC EV relative to control NPC revealed a relatively substantial number ($n = 178$) of unique transcripts differentially expressed in NPC treated with pTGC EV (Figure S10), while $n = 44$ were common to both treatments. A further 44 transcripts were uniquely regulated in NPC treated with EV from TSC. The full list of differentially expressed genes based on the two comparisons, i.e., control NPC versus NPC treated with EV from pTGC and control NPC versus NPC treated with EV from TSC, is provided in Supplementary File S4. The most up- and downregulated transcripts based on fold change in NPC treated with either pTGC- or TSC-derived EV and their known functions are listed in Tables 2 and 3, respectively. The affected genes have been implicated in a wide variety of functions including several processes uniquely associated with neuronal cells. Besides those genes listed in Tables 2 and 3, one transcript of interest that was significantly upregulated in NPC treated with EV from TSC was *Htr2b* (FDR < 0.03), which is one of several receptors for 5-HT (Supplementary File S4) but has been implicated in impulsive behavior in mice [78].

Target enrichment and predicted pathways for differentially expressed transcripts in NPC treated with EV from pTGC and TSC

The TissueEnrich program [58] was then used to determine which organs of the mouse have an abundance of transcripts that are upregulated in NPC exposed to the EV. Upregulated transcripts in NPC treated with EV from pTGC were primarily enriched for transcripts within the brain-specific expression, especially in the cortex and cerebellum (Figure 9A). Elevated transcripts in NPC treated with EV from TSC provided a somewhat similar enrichment for brain-associated transcripts, except for ones associated with the E14.5 fetal brain (Figure 9B). Downregulated transcripts in NPC treated with EV from pTGC had some enrichment for transcripts with brain-specific expression, but those downregulated in NPC treated with EV from TSC had no

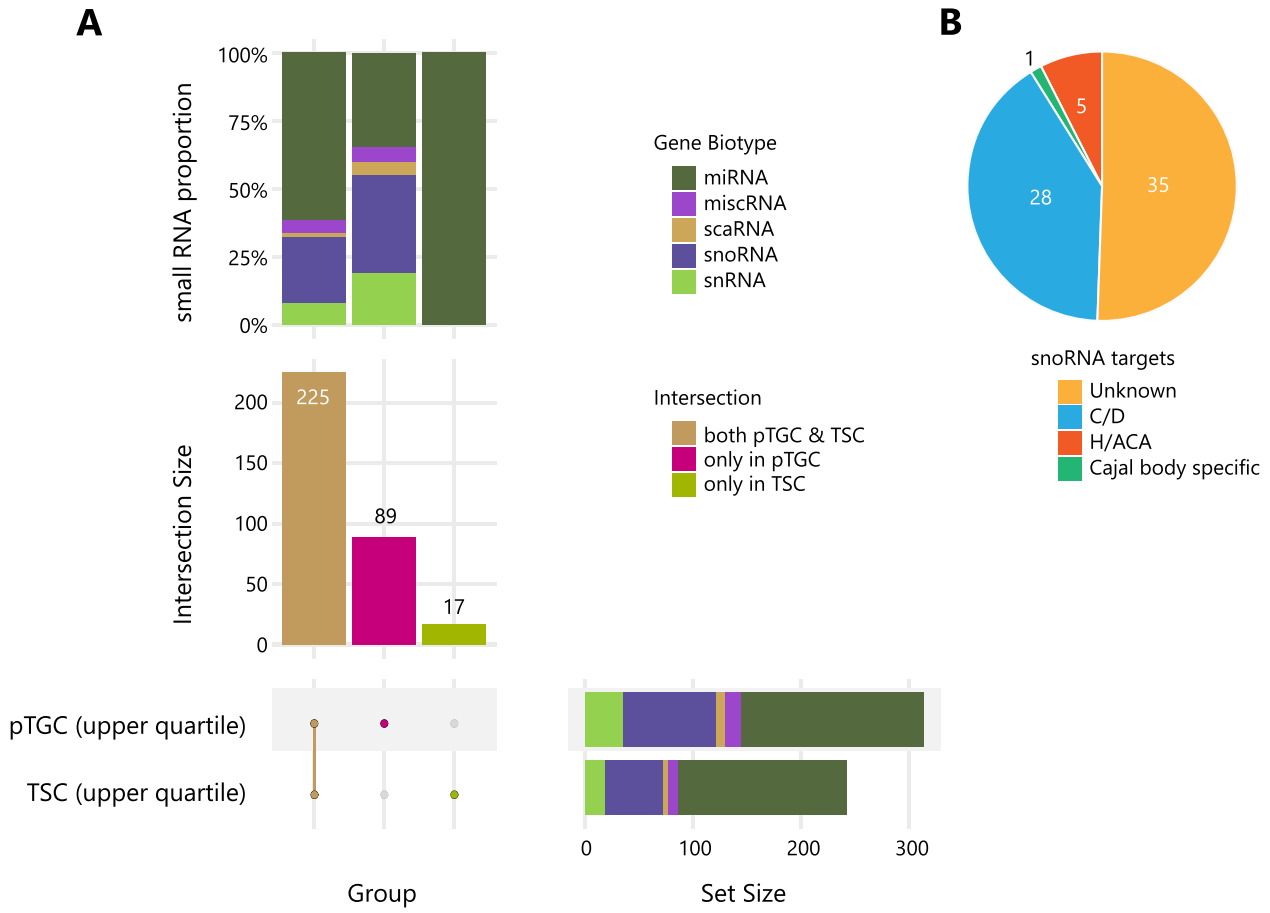

Figure 6. Characterization of the small RNA in EV derived from pTGC vs. TSC. (A) The graphs demonstrate the general composition of the small RNA within these EV. Within the top quartile of the most highly expressed miRNA, 225 overlap in EV derived from pTGC and TSC, 89 are unique to just those from pTGC, and 17 are only detected in EV from TSC. SnoRNA and miRNA are abundant in EV from pTGC. In contrast, miRNA are the primary small RNA within EV from TSC. In the top quartile, TSC EV do not contain any snoRNA that are not in the top quartile of miRNA expressed in pTGC EV. (B) This pie chart shows the composition of snoRNA differentially expressed in EV from pTGC.

Table 2. Top five most up- and downregulated transcripts in NPC treated with EV from pTGC based on fold change with a p-adj ≤0.05

Gene Symbol	Fold change (no EV vs. TSC EV treatment)	p-adj	General function of the encoded protein
Most upregulated transcripts			
Foxp2	4.12	0.0001185	Encodes a member of the forkhead/winged-helix (FOX) family of transcription factors and involved in synapse formation
Tmc3	3.92	0.0001254	Involved in ion transmembrane transport.
Gimap8	3.70	0.0359043	Encodes a protein belonging to the GTP-binding superfamily
Muc2	3.65	0.0064830	Member of the mucin protein family.
Rgs14	3.49	0.0111256	Regulates G protein-coupled receptor signaling cascades
Most downregulated transcripts			
Ndrg2	2.49	0.0000899	Protein encoded by this gene is a cytoplasmic protein that may play a role in neurite outgrowth
Ssc4d	2.33	0.0399908	Scavenger receptor cysteine-rich (SRCR) superfamily
C2cd4c	2.01	0.0217921	Cytosolic protein
Lrrtm1	1.99	0.0112949	Leucine-Rich Repeat Transmembrane Neuronal Protein 1
Pkhd1	1.98	0.0001729	Regulates cellular symmetry by ensuring correct bipolar cell division through the regulation of centrosome duplication and mitotic spindle assembly

significant enrichment for transcripts with tissue-specific expression.

KEGG pathway analysis was used to determine which pathways were likely to have been affected by exposure to the EV (Figure 9C and D). Although there are some clear differences in responses, a number of pathways, for example, calcium signaling, Gap junctions, and circadian entrainment, were common to both treatments. Overall, many of the

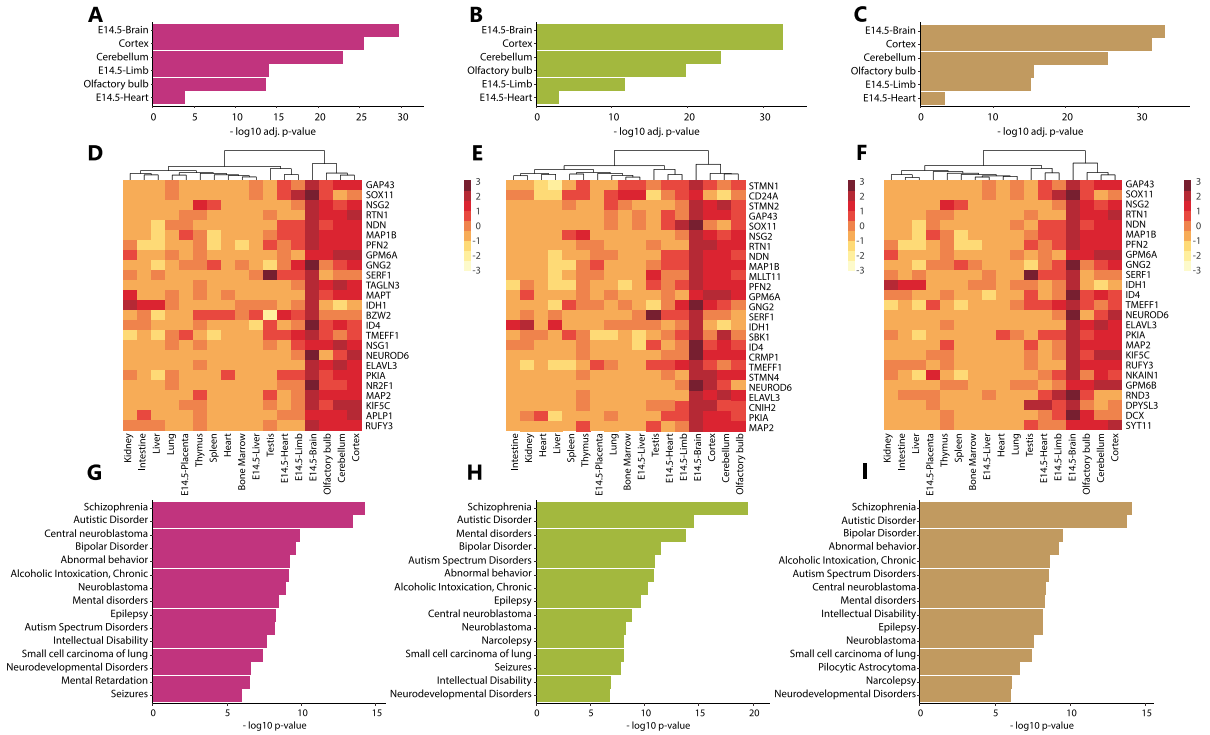

Figure 7. TissueEnrich, heatmap analyses, and diseases associated with predicted mRNA targets, for miRNA within EV from pTGC and TSC. (A) The mRNA targets for upregulated miRNA within EV from pTGC are enriched for genes with tissue-specific expression in the embryonic brain, cerebellum, cerebral cortex, olfactory bulbs, embryonic limb, and embryonic heart. (B) The mRNA targets for upregulated miRNA within EV from TSC are enriched for genes with tissue-specific expression in the embryonic brain, cerebral cortex, cerebellum, olfactory bulb, embryonic limb, and embryonic heart. (C) The overlapping mRNA targets for upregulated miRNA within EV from both pTGC and TSC are enriched for genes with tissue-specific expression in the embryonic brain, cerebral cortex, cerebellum, olfactory bulb, embryonic limb, and embryonic heart. (D) Top predicted mRNA targets enriched in the embryonic brain affected by upregulated miRNA within EV from pTGC. (E) Top mRNA targets enriched in the embryonic brain affected by upregulated miRNA within EV from TSC. (F) Top overlapping mRNA targets within the embryonic brain predicted to be affected by upregulated miRNA within EV derived from both pTGC and TSC. A list of all mRNA targets that have brain-specific expression is included in Dataset S3. Diseases associated with target mRNA for miRNA within EV from (G) pTGC, (H) TSC, and (I) both pTGC and TSC. To determine if the mRNA targets differentially expressed miRNA with EV from pTGC and TSC, we used the DisGeNET (version 7.0) database [68] to screen for potential human-relevant diseases associated with such target mRNA.

pathways are characteristic of both normal and abnormal brain function.

Relationship of miRNA present in EV from pTGC and TSC to up- and downregulated genes in exposed NPC

We checked for matches between targets of the most highly expressed (top quartile) miRNA present in the EV and the genes that were differentially expressed in NPC in response to exposure to EV. Of the miRNA in the top quartile, 95 were predicted to target 54 genes that were differentially expressed in NPC in response to exposure to EV from TSC (46 upregulated in TSC EV treated, and 8 downregulated) (Supplementary File S5). A total of 133 of the top quartile miRNA from pTGC EV were predicted to target 121 genes that were differentially expressed in NPC in response to EV (98 upregulated in pTGC EV treated and 23 downregulated) (Supplementary File S5). The top targets that were upregulated in EV-treated NPC, which also have brain-specific expression, are shown in Table 4. The primary transcripts in EV-treated NPC that demonstrated possible complementarity with miRNA in EV from both pTGC and TSC included *Foxp2* and *Gpr156*. Most of the matches, however, involved transcripts regulated in response to EV from pTGC rather than TSC, for example, *Sema3f*. The general function of almost all of these genes is in regulating neuronal functions, such as synaptogenesis, axon formation, myelination, and voltage-gated channels.

Discussion

An important goal of the current work has been to characterize and compare the protein, catecholamine, and small RNA contents of EV released from mouse pTGC generated in vitro and their progenitor TSC. This study was based on the hypothesis that EV released by pTGC are crucial components of the placenta–brain axis and likely to carry a cargo of bioactive compounds destined to influence brain development in the fetus. We assume that the TB-derived EV reach the brain via the vascular route, with their membrane-shell protecting their contents from catabolism during transit. We then speculate that some form of transcytosis delivers the EV from maternal capillaries to their ultimate targets [79]. Although conceptually vague, this same puzzle concerning mechanism of delivery exists even for studies on the effects of EV on the adult brain [80]. Another unknown is when the blood–brain barrier actually becomes effective during pregnancy in the mouse, although it is probably around E12 [81], possibly after the requirement for placental intervention has expired. Despite these concerns, we believe that the data provided here

Table 3. Top five most up- and downregulated transcripts in NPC treated with EV from TSC based on fold change with a p-adj ≤0.05

Gene Symbol	Fold change (no EV vs. TSC EV treatment)	p-adj	General function of the encoded protein
Most upregulated transcripts			
Slc2a4	3.21	0.0388873	Insulin-regulated facilitative glucose transporter that reduces circulating glucose
Tm4sf20	2.90	0.0212208	Regulates cell proliferation, motility, and adhesion through interactions with integrins.
Lrrc71	2.83	0.0320412	Leucine-Rich Repeat-Containing Protein 71
Arhgef6	2.82	0.0018291	Rho GTPases that regulates diverse cellular processes
Foxp2	2.73	0.0269562	Encodes a member of the forkhead/winged-helix (FOX) family of transcription factors and involved in synapse formation
Most downregulated transcripts			
Zfp983	1.87	0.0188869	Zinc finger protein that regulates transcription
Gja5	1.86	0.0080693	Gap junction protein that regulates cell–cell communication
Pdk1	1.74	0.0000005	Kinase that regulates glucose and fatty acid metabolism by inducing phosphorylation of the pyruvate dehydrogenase subunits PDHA1 and PDHA2
Pkhd1	1.73	0.0064847	Regulates cellular symmetry by ensuring correct bipolar cell division through the regulation of centrosome duplication and mitotic spindle assembly
Samd12	1.73	0.0025995	Involved in transmembrane receptor protein tyrosine kinase signaling pathway

Table 4. Overlap between targets of top quartile most highly expressed miRNA and genes upregulated in EV from pTGC or TSC that have brain-specific expression

Differentially expressed mRNA in NPC	Primary role of protein encoded by transcript in NPC	Fold increase in NPC treated with EV from pTGC (or TSC)	miRNAs targeting the genes in EV from pTGC	miRNAs targeting the genes in EV from mTSC
Foxp2	Regulates synaptogenesis	4.12 (2.67)	mmu-mir-132, mmu-mir-190b, mmu-mir-212, mmu-mir-23a, mmu-mir-23b, mmu-mir-450b, mmu-mir-493, mmu-mir-495, mmu-mir-499	mmu-mir-132, mmu-mir-190b, mmu-mir-212, mmu-mir-23a, mmu-mir-23b, mmu-mir-450b, mmu-mir-495, mmu-mir-499
Gpr156	*Associated with G protein-coupled receptor activity and G protein-coupled GABA receptor activity*	3.25 (1.97)	mmu-let-7g, mmu-mir-185, mmu-mir-98	mmu-let-7g, mmu-mir-185, mmu-mir-98
KIf26b	Associated with microtubules	1.74	mmu-mir-29a	
Sema3f	Regulates axon guidance during neuronal development	1.51	mmu-mir-200b, mmu-mir-200c	
Cacna1h	Voltage-dependent calcium channel complex	1.60	mmu-mir-32, mmu-mir-92b	
Ephb2	*Transferase activity, transferring phosphorus-containing groups and protein tyrosine kinase activity*	2.36	mmu-mir-185, mmu-mir-1968	
Drp2	Regulates myelination	1.53	mmu-mir-130b, mmu-mir-144	
Ptpn5	Regulates molecules essential in synaptic plasticity and neuronal cell survival, including MAPKs, Src family kinases, and NMDA receptors	1.63	mmu-mir-744	
Tvp23a	Membrane protein associated with the Golgi apparatus and regulates intracellular vesicular transport	1.52	mmu-mir-669h	
Kcne2	Voltage-gated potassium channels	2.77	mmu-mir-186, mmu-mir-26a-2, mmu-mir-26b	
Fam167a	Activates the noncanonical NF-κB pathway	1.80	mmu-mir-132, mmu-mir-212, mmu-mir-29a	

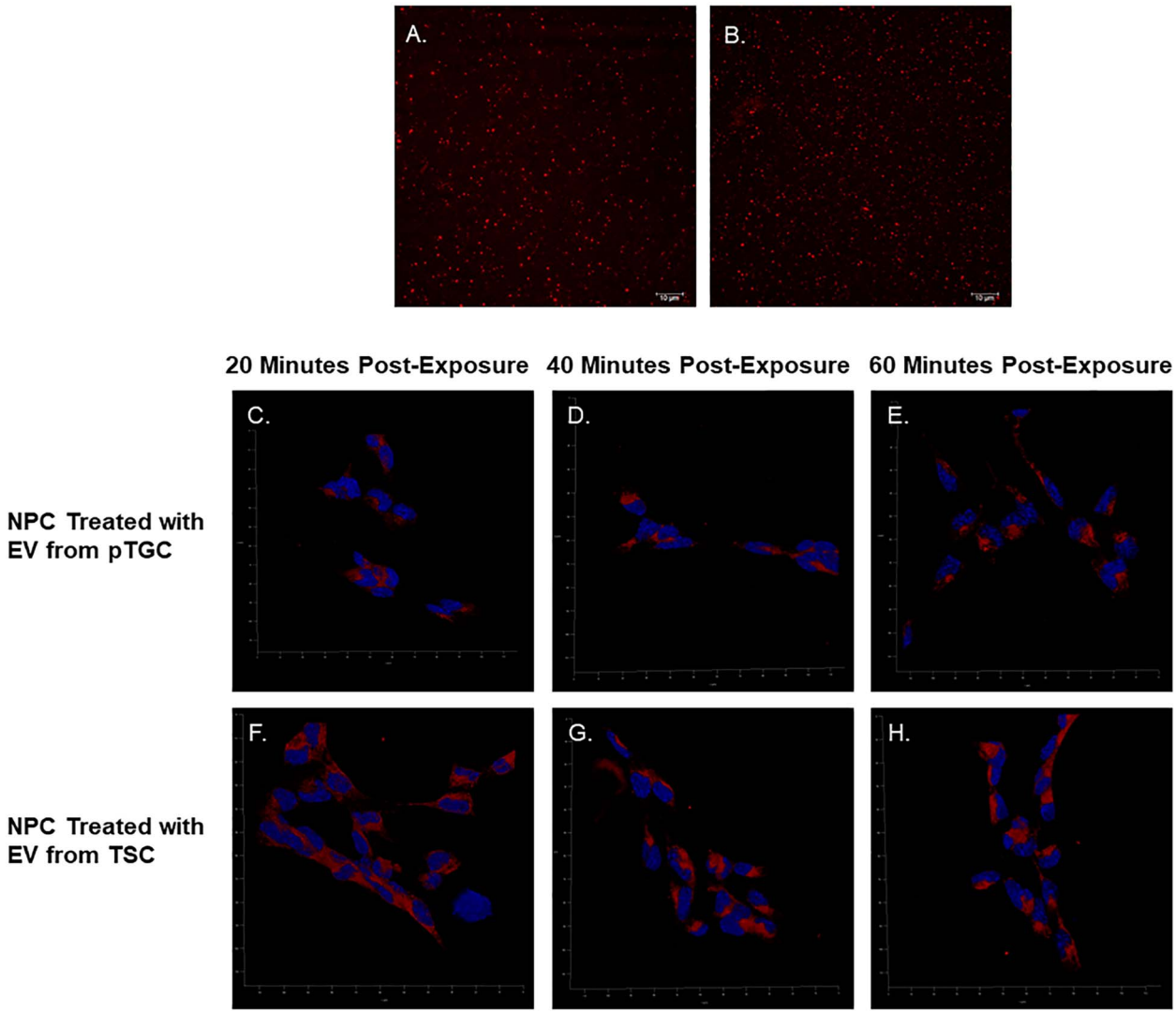

Figure 8. Confocal fluorescent microscopy images showing isolated and fluorescently labeled EV from pTGC and TSC and internalization of TB-derived EV by mouse NPC. (A) Isolated and fluorescently labeled EV from pTGC. (B) Isolated and fluorescently labeled EV from TSC. (C–E) NPC with EV derived from pTGC. (F–H) NPC with EV derived from TSC.

present a case for the ability of the placenta to directly affect development of the fetal brain.

In the Introduction, we discussed the fact that most research on placental EV has been focused on effects elicited on the mother [32–47], while very little has emphasized effects on the fetus, although it has been hypothesized that placental exosomes derived from a diseased placenta may stimulate acute and chronic inflammation and lead to fetal brain damage [82]. To appreciate how placenta-derived EV might affect the fetal brain and other organs, it is first essential to know what they contain.

Scant amount is known about the protein content of TB-derived EV. Proteomics analysis of EV from pTGC and TSC revealed several cytokeratins, tubulins, actins, and heat shock proteins (Figures S3, S4, and S5), which are typical components of EV derived from a variety of sources [83–85]. That, plus the electron microscopic evidence (Figure S3), indicated that we were dealing with bona fide EV. In pTGC EV, there was also significant enrichment of proteins associated primarily with liver-specific gene expression. We have no evidence to date whether or not any of these proteins would be predicted to influence fetal brain or any other targeted organ.

The EV from both sources contained significant amounts of 5-HT, a monoamine neurotransmitter, which, as detailed earlier, influences almost all essential neurological processes in the mouse fetal brain [3–5]. Most recently, 5-HT has been shown to induce gene expression changes in astrocytes in the mouse olfactory bulb by direct biochemical modification (serotonylation) of histones, including those associated with the gene encoding the low-affinity, high-capacity 5-HT transporter (*Slc22a3*) [86]. During early organogenesis in mice, the placenta appears to be a primary source of 5-HT for the fetal brain, whether indirectly via transport from the mother [8, 16, 24] or from direct synthesis in TB [10, 14, 23, 25, 26]. The pTGC have been suggested to be the primary purveyors of this 5-HT [20]. Hence, we predicted at the outset that EV derived from differentiated TSC, i.e., pTGC, would contain greater concentrations than EV from the progenitor TSC. However, no such difference was observed (Figure 3), suggesting that other options must be explored. As dopamine

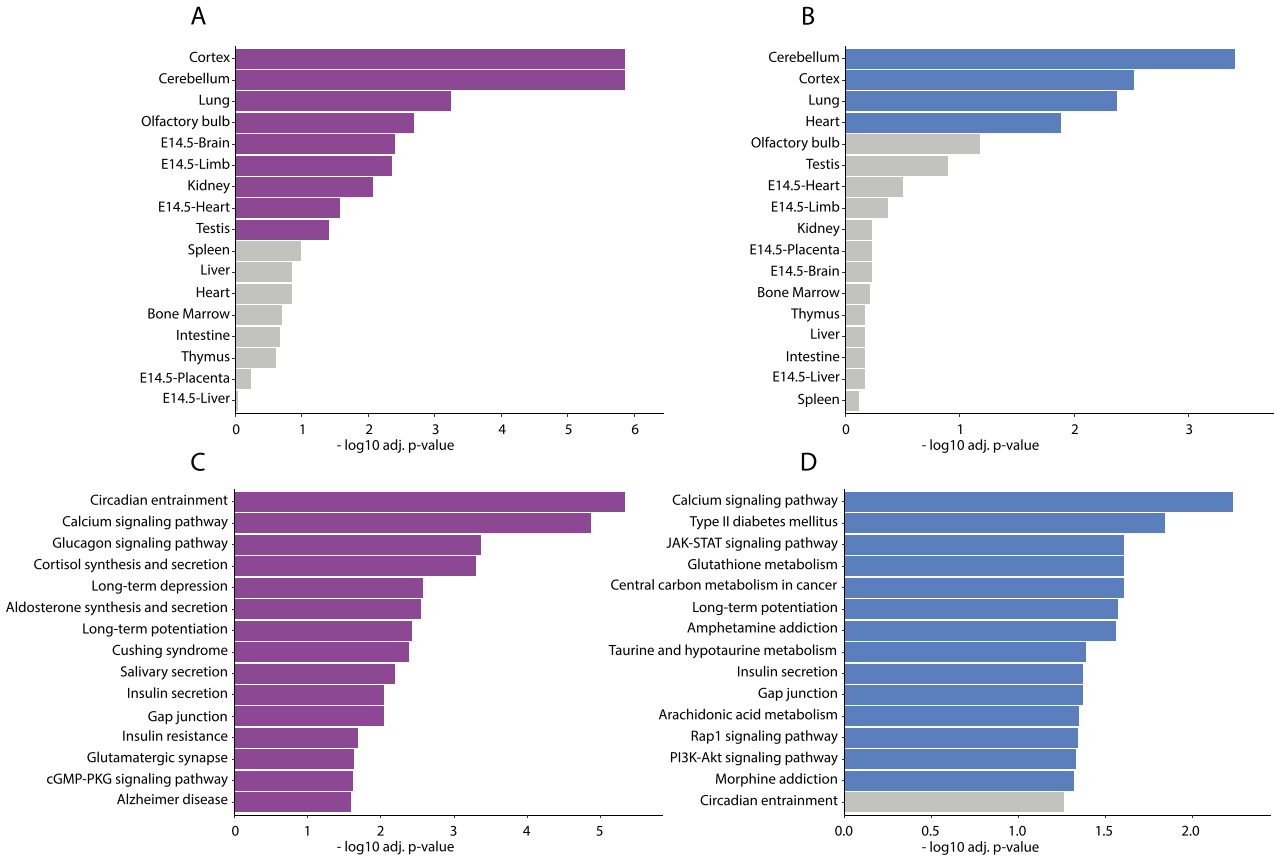

Figure 9. TissueEnrich for transcripts upregulated in NPC treated with EV from pTGC or TSC and predicted KEGG pathways likely to be affected in NPC treated with EV from pTGC or TSC. (A) TissueEnrich analysis for upregulated genes in NPC treated with EV from pTGC. (B) TissueEnrich analysis in genes upregulated for NPC treated with EV from TSC. In both cases, differentially expressed transcripts are predicted to be enriched in various brain regions and olfactory bulb, and embryonic brain in the case of EV from pTGC. (C) Primary pathways likely to be targeted in NPC treated with EV from pTGC include circadian entrainment, calcium signaling pathway, glucagon signaling pathway, cortisol synthesis and secretion, long-term depression, aldosterone synthesis and secretion, long-term potentiation, Cushing syndrome, salivary secretion, insulin secretion, gap junction, insulin resistance, glutamatergic synapse, cGMP–PKG signaling pathway, and Alzheimer disease. (D) Pathways predicted to be affected in NPC exposed to TSC-derived EV include calcium signaling pathway, type II diabetes mellitus, JAK–STAT signaling pathway, glutathione metabolism, central carbon metabolism in cancer, long-term potentiation, amphetamine addiction, taurine and hypotaurine metabolism, insulin secretion, gap junction, arachidonic acid metabolism, Rap1 signaling pathway, morphine addiction, and circadian entrainment.

also accumulates in pTGC in vivo at comparable levels to 5-HT [20], we had also anticipated that it would be present in similar amounts to 5-HT in EV shed from pTGC, but it was present in much lower concentrations. The metabolism and transport of catecholamines in mouse placental TB cells and placenta and the effects of 5-HT on gene expression in NPC clearly warrants further study. Nonetheless, these are the first data to show that EV released from mouse TB cells contain physiologically meaningful concentrations of 5-HT. Previously, low concentrations of 5-HT, choline, and γ-amino butyric acid (GABA) were detected in size-sorted EV isolated from the plasma of both normal individuals and patients suffering from substance abuse disorders [87]. Of particular relevance to our work, the authors observed that levels of several miRNA in the EV were correlated with the severity of anxiety and depression of the patients and with the concentrations of the neurotransmitters. Importantly, some of the miRNA potentially targeted signaling pathways linked to developmental and intellectual abnormalities. As discussed below, these data have parallels to our analysis of the small RNA profiles of EV from mouse TSC and pTGC.

We were first drawn to examining the possible role of small RNA in the placenta–brain axis after discovering that developmental exposure to the endocrine-disrupting chemical bisphenol A altered placental miRNA profiles [27] while also influencing subsequent offspring behavior [88–91]. To our surprise, we discovered that the target mRNA for these whole placental EV were the ones enriched in the thymus and various neural tissues but not the placenta [27], suggesting possible roles of placental miRNA in controlling maternal immune responses and brain neurobiology rather than placental development. Work from other laboratories has likewise suggested that placental miRNA might contribute to fetal brain development in the mouse [28] and human [29, 30]. In our present work with cultured TB cells, miRNA formed about two-thirds of the small RNA found in EV from the TSC and about one-third from pTGC (Figure 6). In addition, while levels of many individual miRNA did not differ significantly between EV type, others showed a more preferred association with one EV type relative to the other (Figure 6; Table 1). Strikingly, many of the miRNA, especially those from pTGC, had, as potential targets, transcripts with tissue-specific expression in the E14.5 mouse brain and component tissues (Figure 7). Together, these data are consistent with the possibility that the cargo carried from TSC and pTGC is destined primarily for the fetal brain. Moreover, many of the miRNA present in EV from pTGC and

TSC have been implicated in neurodevelopmental disorders, including ASD (Figure 7).

While the miRNA analyses revealed many similarities between the EV from TSC and their differentiated product, the pTGC, the snoRNA were much more abundant in pTGC-derived EV. SnoRNA are defined as a sub-type of snRNA that are generally present in introns as clusters. Ascribed functions include modification of other RNA and alterations in protein expression. They can also be precursors of other small RNA types [92]. Based on their motif, snoRNA may induce DNA methylation (C/D box motif) or pseudouridylation (H/ACA box motif) [93]. As shown in Figure 6, both types are upregulated in pTGC-derived EV. They have been described in placenta [92], but little is known about their roles, although in other systems they have been reported to affect the expression of neuronal-associated genes [94]. In addition, allelic imbalance and dysregulation of orphan C/D box snoRNA has been implicated in some forms of autism spectrum disorders (ASD) [95]. If snoRNA originating from the placenta function as contributory factors to ASD, they might be useful as early diagnostic biomarkers. Clearly, further research on these enigmatic molecules is warranted.

Extracellular vesicles from both pTGC and TSC were readily taken up by cultured NPC (Figure 8). RNAseq analysis performed 24 h after initial exposure revealed that EV from each TB cell type induced distinct gene signature patterns in NPC (Figure S9). Analysis of the differentially regulated genes from both treatments for tissue enrichment showed that the transcript profiles reflected brain cortex and cerebellum and, in the case of EV from pTGC, the mouse E14.5 brain (Figure 9), suggesting that the pTGC might induce gene-sets associated with early neurogenesis. One gene whose expression was significantly altered in NPC treated with TSC EV was *Htr2b* (Figure S9), which encodes for 5-Hydroxytryptamine Receptor 2B protein that binds 5-HT and has been implicated as associated with bipolar disorder [96]. Although not significant, counts for this gene also appear increased in NPC treated with pTGC EV (Figure S11). Thus, EV from TSC and pTGC may enhance NPC responses to 5-HT.

In our final set of analyses, we examined the genes whose expression had changed most based on fold change in NPC exposed to EV and whether their transcripts could be potential targets for the miRNA that had been delivered to the NPC via the EV (Supplementary File S5 and Table 4). We came to two conclusions. The first was that the functions of the regulated transcripts that demonstrated the strongest complementary to miRNA in the EV are linked to neuronal functions, such as synaptogenesis, axon formation, myelination, and voltage-gated channels. Second, the NPC transcripts with strongest matches to EV miRNA were up- rather than downregulated, a somewhat surprising outcome. However, there are examples of miRNA amplifying gene expression [97–101] (Supplementary File S4 and Table 1). Whatever the mechanism, these data provide convincing evidence that miRNA delivered by EV derived from pTGC and TSC affect gene expression by NPC.

In conclusion, the current studies have characterized the protein, catecholamine, and small RNA content of EV released from TSC and pTGC of the mouse. Protein and small RNA differed depending on the source of the EV. However, no concentration differences in 5-HT, dopamine, and norepinephrine were detected between EV sources. 5-Hydroxytryptamine, in particular, was present in amounts that could conceivably affect fetal brain development. The EV, in addition, contained several kinds of small RNA. The inferred primary targets of the miRNA from both TSC and pTGC were mRNA enriched in the fetal brain, providing support for the notion that placenta-derived miRNA contained within EV vectors shuttle their cargo to the emerging brain. SnoRNA were upregulated in EV from pTGC relative to TSC, and these molecules might also be expected to influence the expression of neuroregulatory genes. Mouse NPC internalize EV from pTGC and TSC and respond by changes in their transcriptome profiles. MicroRNA within EV from pTGC and TSC have as potential targets several upregulated NPC transcripts, suggesting that these miRNA could be positive regulators of gene expression. Placenta-derived EV, therefore, might hold the key to understanding neurobehavioral disorders that arise from disruptions in the placenta–brain axis.

Acknowledgment

We are grateful to Dr. Neil Hunter and HHMI for funding the LC–MS work. We are also grateful to the members of the Rosenfeld and Roberts' laboratories who assisted with these studies. We appreciate Dr. Haifan Lin's (Yale University) input and analysis of the snoRNA data.

Conflict of Interest

The authors have declared that no conflict of interest exists.

Author Contributions

JAK, SS, and NJB performed the experiments. ASS, BSP, GG, and GT analyzed the proteomics and small RNAseq data for EV from pTGC and TSC and RNAseq data from NPC treated with EV from pTGC and TSC. JAK, SS, RMR, and CSR designed the experiments. JAK, ASS, SS, NJB, BSP, GG, RMR, GT, and CSR wrote and edited the manuscript and helped prepare the figure, tables, and supplemental files.

Data Availability

Proteomics data are available at http://massive.ucsd.edu/ProteoSAFe/status.jsp?task=35b93125f20f40ebbae166e5f8657860. The GitHub repository documenting all the small RNA sequencing analysis steps and the custom R scripts used in this study are available at https://github.com/Tuteja-Lab/mouse.trophoblast.smallRNAseq. Small RNA sequencing data have been deposited in the Gene Expression Omnibus under accession ID GSE222855. The mRNA sequencing data from mouse NPC have been deposited into the Gene Expression Omnibus under accession ID GSE230783.

Supplementary Data

Supplementary data are available at *BIOLRE* online.

References

1. Rosenfeld CS. Placental serotonin signaling, pregnancy outcomes, and regulation of fetal brain development†. *Biol Reprod* 2020; **102**:532–538.
2. Rosenfeld CS. The placenta-brain-axis. *J Neurosci Res* 2021; **99**: 271–283.
3. Chubakov AR, Gromova EA, Konovalov GV, Sarkisova EF, Chumasov EI. The effects of serotonin on the morpho-functional development of rat cerebral neocortex in tissue culture. *Brain Res* 1986; **369**:285–297.
4. Chumasov EI, Chubakov AR, Konovalov GV, Gromova EA. Effect of serotonin on growth and differentiation of hippocampal cells in culture. *Neurosci Behav Physiol* 1980; **10**:125–131.

5. Gromova HA, Chubakov AR, Chumasov EI, Konovalov HV. Serotonin as a stimulator of hippocampal cell differentiation in tissue culture. *Int J Dev Neurosci* 1983; **1**:339–349.
6. Koren Z, Pfeifer Y, Sulman FG. Serotonin content of human placenta and fetus during pregnancy. *Am J Obstet Gynecol* 1965; **93**:411–415.
7. Laurent L, Deroy K, St-Pierre J, Côté F, Sanderson JT, Vaillancourt C. Human placenta expresses both peripheral and neuronal isoform of tryptophan hydroxylase. *Biochimie* 2017; **140**: 159–165.
8. Kliman HJ, Quaratella SB, Setaro AC, Siegman EC, Subha ZT, Tal R, Milano KM, Steck TL. Pathway of maternal serotonin to the human embryo and fetus. *Endocrinology* 2018; **159**:1609–1629.
9. Vaillancourt C, Petit A, Gallo-Payet N, Bellabarba D, Lehoux JG, Belisle S. Labelling of D2-dopaminergic and 5-HT2-serotonergic binding sites in human trophoblastic cells using [3H]-spiperone. *J Recept Res* 1994; **14**:11–22.
10. Huang WQ, Zhang CL, Di XY, Zhang RQ. Studies on the localization of 5-hydroxytryptamine and its receptors in human placenta. *Placenta* 1998; **19**:655–661.
11. Viau M, Lafond J, Vaillancourt C. Expression of placental serotonin transporter and 5-HT 2A receptor in normal and gestational diabetes mellitus pregnancies. *Reprod Biomed Online* 2009; **19**:207–215.
12. Hadden C, Fahmi T, Cooper A, Savenka AV, Lupashin VV, Roberts DJ, Maroteaux L, Hauguel-de Mouzon S, Kilic F. Serotonin transporter protects the placental cells against apoptosis in caspase 3-independent pathway. *J Cell Physiol* 2017; **232**: 3520–3529.
13. Wu HH, Choi S, Levitt P. Differential patterning of genes involved in serotonin metabolism and transport in extra-embryonic tissues of the mouse. *Placenta* 2016; **42**:74–83.
14. Tuteja G, Chung T, Bejerano G. Changes in the enhancer landscape during early placental development uncover a trophoblast invasion gene-enhancer network. *Placenta* 2016; **37**:45–55.
15. Vu HTH, Kaur H, Kies KR, Starks RR, Tuteja G. Identifying novel regulators of placental development using time-series transcriptome data. *Life Science Alliance* 2023; **6**:e202201788.
16. Yavarone MS, Shuey DL, Sadler TW, Lauder JM. Serotonin uptake in the ectoplacental cone and placenta of the mouse. *Placenta* 1993; **14**:149–161.
17. Latos PA, Hemberger M. From the stem of the placental tree: trophoblast stem cells and their progeny. *Development* 2016; **143**:3650–3660.
18. Hu D, Cross JC. Development and function of trophoblast giant cells in the rodent placenta. *Int J Dev Biol* 2010; **54**: 341–354.
19. Natale BV, Schweitzer C, Hughes M, Globisch MA, Kotadia R, Tremblay E, Vu P, Cross JC, Natale DRC. Sca-1 identifies a trophoblast population with multipotent potential in the mid-gestation mouse placenta. *Sci Rep* 2017; **7**:5575.
20. Mao J, Jain A, Denslow ND, Nouri MZ, Chen S, Wang T, Zhu N, Koh J, Sarma SJ, Sumner BW, Lei Z, Sumner LW, *et al.* Bisphenol a and bisphenol S disruptions of the mouse placenta and potential effects on the placenta-brain axis. *Proc Natl Acad Sci U S A* 2020; **117**:4642–4652.
21. Hannibal RL, Baker JC. Selective amplification of the genome surrounding key placental genes in trophoblast Giant cells. *Curr Biol* 2016; **26**:230–236.
22. Simmons DG, Fortier AL, Cross JC. Diverse subtypes and developmental origins of trophoblast giant cells in the mouse placenta. *Dev Biol* 2007; **304**:567–578.
23. Bonnin A, Goeden N, Chen K, Wilson ML, King J, Shih JC, Blakely RD, Deneris ES, Levitt P. A transient placental source of serotonin for the fetal forebrain. *Nature* 2011; **472**:347–350.
24. Cote F, Fligny C, Bayard E, Launay JM, Gershon MD, Mallet J, Vodjdani G. Maternal serotonin is crucial for murine embryonic development. *Proc Natl Acad Sci U S A* 2007; **104**:329–334.
25. Bonnin A, Levitt P. Fetal, maternal, and placental sources of serotonin and new implications for developmental programming of the brain. *Neuroscience* 2011; **197**:1–7.
26. Muller CL, Anacker AM, Rogers TD, Goeden N, Keller EH, Forsberg CG, Kerr TM, Wender C, Anderson GM, Stanwood GD, Blakely RD, Bonnin A, *et al.* Impact of maternal serotonin transporter genotype on placental serotonin, fetal forebrain serotonin, and neurodevelopment. *Neuropsychopharmacology* 2017; **42**:427–436.
27. Mao J, Kinkade JA, Bivens NJ, Rosenfeld CS. miRNA changes in the mouse placenta due to bisphenol a exposure. *Epigenomics* 2021; **13**:1909–1919.
28. Strawn M, Samal A, Sarker MB, Dhakal P, Behura SK. Relevance of microRNAs to the regulation of the brain-placental axis in mice. *Placenta* 2021; **112**:123–131.
29. Lackinger M, Sungur A, Daswani R, Soutschek M, Bicker S, Stemmler L, Wüst T, Fiore R, Dieterich C, Schwarting RK, Wöhr M, Schratt G. A placental mammal-specific microRNA cluster acts as a natural brake for sociability in mice. *EMBO Rep* 2019; **20**:e46429.
30. Santos HP Jr, Bhattacharya A, Joseph RM, Smeester L, Kuban KCK, Marsit CJ, O'Shea TM, Fry RC. Evidence for the placenta-brain axis: multi-omic kernel aggregation predicts intellectual and social impairment in children born extremely preterm. *Mol Autism* 2020; **11**:97.
31. Mashouri L, Yousefi H, Aref AR, Am A, Molaei F, Alahari SK. Exosomes: composition, biogenesis, and mechanisms in cancer metastasis and drug resistance. *Mol Cancer* 2019; **18**:75.
32. Ayala-Ramírez P, Machuca-Acevedo C, Gámez T, Quijano S, Barreto A, Silva JL, Olaya CM, García-Robles R. Assessment of placental extracellular vesicles-associated Fas ligand and TNF-related apoptosis-inducing ligand in pregnancies complicated by early and late onset preeclampsia. *Front Physiol* 2021; **12**:708824.
33. Buca D, Bologna G, D'Amico A, Cugini S, Musca F, Febbo M, D'Arcangelo D, Buca D, Simeone P, Liberati M, Vitacolonna E, Miscia S, *et al.* Extracellular vesicles in feto-maternal crosstalk and pregnancy disorders. *Int J Mol Sci* 2020; **21**: 2120.
34. Czernek L, Düchler M. Exosomes as messengers between mother and fetus in pregnancy. *Int J Mol Sci* 2020; **21**:4264.
35. Gebara N, Correia Y, Wang K, Bussolati B. Angiogenic properties of placenta-derived extracellular vesicles in normal pregnancy and in preeclampsia. *Int J Mol Sci* 2021; **22**:5402.
36. Hashimoto A, Sugiura K, Hoshino A. Impact of exosome-mediated feto-maternal interactions on pregnancy maintenance and development of obstetric complications. *J Biochem* 2021; **169**:163–171.
37. James-Allan LB, Devaskar SU. Extracellular vesicles and their role in gestational diabetes mellitus. *Placenta* 2021; **113**:15–22.
38. Kupper N, Huppertz B. The endogenous exposome of the pregnant mother: placental extracellular vesicles and their effect on the maternal system. *Mol Aspects Med* 2021;**87**:100955.
39. Morales-Prieto DM, Favaro RR, Markert UR. Placental miRNAs in feto-maternal communication mediated by extracellular vesicles. *Placenta* 2020; **102**:27–33.
40. Nair S, Guanzon D, Jayabalan N, Lai A, Scholz-Romero K, Kalita de Croft P, Ormazabal V, Palma C, Diaz E, McCarthy EA, Shub A, Miranda J, *et al.* Extracellular vesicle-associated miRNAs are an adaptive response to gestational diabetes mellitus. *J Transl Med* 2021; **19**:360.
41. Nair S, Salomon C. Extracellular vesicles as critical mediators of maternal-fetal communication during pregnancy and their potential role in maternal metabolism. *Placenta* 2020; **98**:60–68.
42. Palma C, Jellins J, Lai A, Salas A, Campos A, Sharma S, Duncombe G, Hyett J, Salomon C. Extracellular vesicles and preeclampsia: current knowledge and future research directions. *Subcell Biochem* 2021; **97**:455–482.

43. Rajaratnam N, Ditlevsen NE, Sloth JK, Bæk R, Jørgensen MM, Christiansen OB. Extracellular vesicles: an important biomarker in recurrent pregnancy loss? *J Clin Med* 2021; **10**:2549.
44. Tang Y, Groom K, Chamley L, Chen Q. Melatonin, a potential therapeutic agent for preeclampsia, reduces the extrusion of toxic extracellular vesicles from preeclamptic placentae. *Cell* 2021; **10**:1904.
45. Tersigni C, Lucchetti D, Franco R, Colella F, Neri C, Crispino L, Sgambato A, Lanzone A, Scambia G, Vatish M, Di Simone N. Circulating placental vesicles carry HLA-DR in pre-eclampsia: a new potential marker of the syndrome. *Front Immunol* 2021; **12**:717879.
46. Wang L, Zhang W, Zou N, Zhang L. Trophoblasts modulate the Ca(2+) oscillation and contraction of myometrial smooth muscle cells by small extracellular vesicle- (sEV-) mediated exporting of miR-25-3p during premature labor. *Oxid Med Cell Longev* 2021; **2021**:8140667.
47. Block LN, Bowman BD, Schmidt JK, Keding LT, Stanic AK, Golos TG. The promise of placental extracellular vesicles: models and challenges for diagnosing placental dysfunction in utero†. *Biol Reprod* 2021; **104**:27–57.
48. Yang CJ, Tan HP, Du YJ. The developmental disruptions of serotonin signaling may involved in autism during early brain development. *Neuroscience* 2014; **267**:1–10.
49. Sato K. Placenta-derived hypo-serotonin situations in the developing forebrain cause autism. *Med Hypotheses* 2013; **80**:368–372.
50. Tanaka S, Kunath T, Hadjantonakis AK, Nagy A, Rossant J. Promotion of trophoblast stem cell proliferation by FGF4. *Science* 1998; **282**:2072–2075.
51. Himeno E, Tanaka S, Kunath T. Isolation and manipulation of mouse trophoblast stem cells. *Curr Protoc Stem Cell Biol* 2008; **7**:Unit 1E.4.
52. Morimoto H, Ueno M, Tanabe H, Kono T, Ogawa H. Progesterone depletion results in Lamin B1 loss and induction of cell death in mouse trophoblast giant cells. *PloS One* 2021; **16**:e0254674.
53. Nishitani K, Hayakawa K, Minatomoto M, Tanaka K, Ogawa H, Kojima H, Tanaka S. N-Oleoyldopamine promotes the differentiation of mouse trophoblast stem cells into parietal trophoblast giant cells. *Biochem Biophys Res Commun* 2022; **636**: 205–212.
54. Hemberger M, Hughes M, Cross JC. Trophoblast stem cells differentiate in vitro into invasive trophoblast giant cells. *Dev Biol* 2004; **271**:362–371.
55. Ullah R, Naz A, Akram HS, Ullah Z, Tariq M, Mithani A, Faisal A. Transcriptomic analysis reveals differential gene expression, alternative splicing, and novel exons during mouse trophoblast stem cell differentiation. *Stem Cell Research & Therapy* 2020; **11**:342.
56. Mao J, Kinkade JA, Bivens NJ, Roberts RM, Rosenfeld CS. Placental changes in the serotonin transporter (Slc6a4) knockout mouse suggest a role for serotonin in controlling nutrient acquisition. *Placenta* 2021; **115**:158–168.
57. Shen Y, Yue F, McCleary DF, Ye Z, Edsall L, Kuan S, Wagner U, Dixon J, Lee L, Lobanenkov VV, Ren B. A map of the cis-regulatory sequences in the mouse genome. *Nature* 2012; **488**: 116–120.
58. Jain A, Tuteja G. TissueEnrich: tissue-specific gene enrichment analysis. *Bioinformatics* 2019; **35**:1966–1967.
59. Szklarczyk D, Franceschini A, Wyder S, Forslund K, Heller D, Huerta-Cepas J, Simonovic M, Roth A, Santos A, Tsafou KP, Kuhn M, Bork P, *et al.* STRING v10: protein-protein interaction networks, integrated over the tree of life. *Nucleic Acids Res* 2015; **43**:D447–D452.
60. Chin CH, Chen SH, Wu HH, Ho CW, Ko MT, Lin CY. cytoHubba: identifying hub objects and sub-networks from complex interactome. *BMC Syst Biol* 2014; **8**:S11.
61. Shannon P, Markiel A, Ozier O, Baliga NS, Wang JT, Ramage D, Amin N, Schwikowski B, Ideker T. Cytoscape: a software environment for integrated models of biomolecular interaction networks. *Genome Res* 2003; **13**:2498–2504.
62. Frankish A, Carbonell-Sala S, Diekhans M, Jungreis I, Loveland JE, Mudge JM, Sisu C, Wright JC, Arnan C, Barnes I, Banerjee A, Bennett R, *et al.* GENCODE: reference annotation for the human and mouse genomes in 2023. *Nucleic Acids Res* 2023; **51**:D942–D949.
63. Dobin A, Davis CA, Schlesinger F, Drenkow J, Zaleski C, Jha S, Batut P, Chaisson M, Gingeras TR. STAR: ultrafast universal RNA-seq aligner. *Bioinformatics* 2013; **29**:15–21.
64. Love MI, Huber W, Anders S. Moderated estimation of fold change and dispersion for RNA-seq data with DESeq2. *Genome Biol* 2014; **15**:550.
65. Kolde, R. Pheatmap: pretty heatmaps. *R Package Version 1.0.12*. 2019; https://CRAN.R-project.org/package=pheatmap.
66. Chen Y, Wang X. miRDB: an online database for prediction of functional microRNA targets. *Nucleic Acids Res* 2020; **48**:D127–D131.
67. Liu W, Wang X. Prediction of functional microRNA targets by integrative modeling of microRNA binding and target expression data. *Genome Biol* 2019; **20**:18.
68. Pinero J, Ramirez-Anguita JM, Sauch-Pitarch J, Ronzano F, Centeno E, Sanz F, Furlong LI. The DisGeNET knowledge platform for disease genomics: 2019 update. *Nucleic Acids Res* 2020; **48**:D845–D855.
69. Kanehisa M, Goto S. KEGG: Kyoto Encyclopedia of Genes and Genomes. *Nucleic Acids Res* 2000; **28**:27–30.
70. Kanehisa M. Toward understanding the origin and evolution of cellular organisms. *Protein Sci* 2019; **28**:1947–1951.
71. Andrews S. FastQC A quality control tool for high throughput sequence data. 2010; https://www.bioinformatics.babraham.ac.uk/projects/fastqc/.
72. Ewels P, Magnusson M, Lundin S, Kaller M. MultiQC: summarize analysis results for multiple tools and samples in a single report. *Bioinformatics* 2016; **32**:3047–3048.
73. Love MI, Anders S, Kim V, Huber W. RNA-Seq workflow: gene-level exploratory analysis and differential expression. *F1000Res* 2015; **4**:1070.
74. Benjamini Y, Drai D, Elmer G, Kafkafi N, Golani I. Controlling the false discovery rate: a practical and powerful approach to multiple testing. *J Royal Stat Soc* 1995; **57**:289–300.
75. Luo Y, Hitz BC, Gabdank I, Hilton JA, Kagda MS, Lam B, Myers Z, Sud P, Jou J, Lin K, Baymuradov UK, Graham K, *et al.* New developments on the Encyclopedia of DNA Elements (ENCODE) data portal. *Nucleic Acids Res* 2020; **48**:D882–D889.
76. Xie Z, Bailey A, Kuleshov MV, Clarke DJB, Evangelista JE, Jenkins SL, Lachmann A, Wojciechowicz ML, Kropiwnicki E, Jagodnik KM, Jeon M, Ma'ayan A. Gene set knowledge discovery with Enrichr. *Curr Protoc* 2021; **1**:e90.
77. Pico AR, Kelder T, van Iersel MP, Hanspers K, Conklin BR, Evelo C. WikiPathways: pathway editing for the people. *PLoS Biol* 2008; **6**:e184.
78. Bevilacqua L, Doly S, Kaprio J, Yuan Q, Tikkanen R, Paunio T, Zhou Z, Wedenoja J, Maroteaux L, Diaz S, Belmer A, Hodgkinson CA, *et al.* A population-specific HTR2B stop codon predisposes to severe impulsivity. *Nature* 2010; **468**:1061–1066.
79. Goasdoue K, Miller SM, Colditz PB, Bjorkman ST. Review: The blood-brain barrier; protecting the developing fetal brain. *Placenta* 2017; **54**:111–116.
80. Ramos-Zaldivar HM, Polakovicova I, Salas-Huenuleo E, Corvalan AH, Kogan MJ, Yefi CP, Andia ME. Extracellular vesicles through the blood-brain barrier: a review. *Fluids Barriers CNS* 2022; **19**:60.
81. Delaney C, Campbell M. The blood brain barrier: insights from development and ageing. *Tissue Barriers* 2017; **5**: e1373897.
82. Gall AR, Amoah S, Kitase Y, Jantzie LL. Placental mediated mechanisms of perinatal brain injury: evolving inflammation and exosomes. *Exp Neurol* 2022; **347**:113914.

83. Griffiths SG, Cormier MT, Clayton A, Doucette AA. Differential proteome analysis of extracellular vesicles from breast cancer cell lines by chaperone affinity enrichment. *Proteomes* 2017; **5**:25.
84. Sheller S, Papaconstantinou J, Urrabaz-Garza R, Richardson L, Saade G, Salomon C, Menon R. Amnion-epithelial-cell-derived exosomes demonstrate physiologic state of cell under oxidative stress. *PloS One* 2016; **11**:e0157614.
85. Jeppesen DK, Fenix AM, Franklin JL, Higginbotham JN, Zhang Q, Zimmerman LJ, Liebler DC, Ping J, Liu Q, Evans R, Fissell WH, Patton JG, *et al*. Reassessment of exosome composition. *Cell* 2019; **177**:428, e418–445.
86. Sardar D, Cheng YT, Woo J, Choi DJ, Lee ZF, Kwon W, Chen HC, Lozzi B, Cervantes A, Rajendran K, Huang TW, Jain A, *et al*. Induction of astrocytic Slc22a3 regulates sensory processing through histone serotonylation. *Science* 2023; **380**:eade0027.
87. Chen F, Xu Y, Shi K, Zhang Z, Xie Z, Wu H, Ma Y, Zhou Y, Chen C, Yang J, Wang Y, Robbins TW, *et al*. Multi-omics study reveals associations among neurotransmitter, extracellular vesicle-derived microRNA and psychiatric comorbidities during heroin and methamphetamine withdrawal. *Biomed Pharmacother* 2022; **155**:113685.
88. Jasarevic E, Sieli PT, Twellman EE, Welsh TH Jr, Schachtman TR, Roberts RM, Geary DC, Rosenfeld CS. Disruption of adult expression of sexually selected traits by developmental exposure to bisphenol A. *Proc Natl Acad Sci U S A* 2011; **108**: 11715–11720.
89. Jasarevic E, Williams SA, Vandas GM, Ellersieck MR, Liao C, Kannan K, Roberts RM, Geary DC, Rosenfeld CS. Sex and dose-dependent effects of developmental exposure to bisphenol A on anxiety and spatial learning in deer mice (Peromyscus maniculatus bairdii) offspring. *Horm Behav* 2013; **63**: 180–189.
90. Williams SA, Jasarevic E, Vandas GM, Warzak DA, Geary DC, Ellersieck MR, Roberts RM, Rosenfeld CS. Effects of developmental bisphenol A exposure on reproductive-related behaviors in California mice (*Peromyscus californicus*): a monogamous animal model. *PloS One* 2013; **8**:e55698.
91. Johnson SA, Javurek AB, Painter MS, Ellersieck MR, Welsh TH Jr, Camacho L, Lewis SM, Vanlandingham MM, Ferguson SA, Rosenfeld CS. Effects of developmental exposure to bisphenol a on spatial navigational learning and memory in rats: a CLARITY-BPA study. *Horm Behav* 2016; **80**:139–148.
92. Telkar N, Stewart GL, Pewarchuk ME, Cohn DE, Robinson WP, Lam WL. Small non-coding RNAs in the human placenta: regulatory roles and clinical utility. *Front Genet* 2022; **13**:868598.
93. Liang J, Wen J, Huang Z, Chen XP, Zhang BX, Chu L. Small nucleolar RNAs: insight into their function in cancer. *Front Oncol* 2019; **9**:587.
94. Gong J, Li Y, Liu CJ, Xiang Y, Li C, Ye Y, Zhang Z, Hawke DH, Park PK, Diao L, Putkey JA, Yang L, *et al*. A pan-cancer analysis of the expression and clinical relevance of small nucleolar RNAs in human cancer. *Cell Rep* 2017; **21**:1968–1981.
95. Lee C, Kang EY, Gandal MJ, Eskin E, Geschwind DH. Profiling allele-specific gene expression in brains from individuals with autism spectrum disorder reveals preferential minor allele usage. *Nat Neurosci* 2019; **22**:1521–1532.
96. Medina AA-O, Hagenauer MA-O, Krolewski DM, Hughes EA-OX, Forrester LCT, Walsh DM, Waselus MA-O, Richardson E, Turner CA, Sequeira PA-O, Cartagena PM, Thompson RC, *et al*. Neurotransmission-related gene expression in the frontal pole is altered in subjects with bipolar disorder and schizophrenia. *Transl Psychiatry* 2023; **13**:118.
97. Place RF, Li LC, Pookot D, Noonan EJ, Dahiya R. MicroRNA-373 induces expression of genes with complementary promoter sequences. *Proc Natl Acad Sci U S A* 2008; **105**:1608–1613.
98. Jame-Chenarboo F, Ng HH, Macdonald D, Mahal LK. High-throughput analysis reveals miRNA upregulating α-2,6-sialic acid through direct miRNA–mRNA interactions. *ACS Central Science* 2022; **8**:1527–1536.
99. Truesdell SS, Mortensen RD, Seo M, Schroeder JC, Lee JH, LeTonqueze O, Vasudevan S. MicroRNA-mediated mRNA translation activation in quiescent cells and oocytes involves recruitment of a nuclear microRNP. *Sci Rep* 2012; **2**:842.
100. Bukhari SIA, Truesdell SS, Lee S, Kollu S, Classon A, Boukhali M, Jain E, Mortensen RD, Yanagiya A, Sadreyev RI, Haas W, Vasudevan S. A specialized mechanism of translation mediated by FXR1a-associated MicroRNP in cellular quiescence. *Mol Cell* 2016; **61**:760–773.
101. Ørom UA, Nielsen FC, Lund AH. MicroRNA-10a binds the 5′UTR of ribosomal protein mRNAs and enhances their translation. *Mol Cell* 2008; **30**:460–471.